

Deep Convolutional Framelets: A General Deep Learning for Inverse Problems

Jong Chul Ye*, *Senior Member, IEEE*, and Yo Seob Han

Abstract

Recently, deep learning approaches with various network architectures have achieved significant performance improvement over existing iterative reconstruction methods in various imaging problems. However, it is still unclear *why* these deep learning architectures work for specific inverse problems. Moreover, unlike the usual evolution of signal processing theory around the classical theories, the link between the deep learning and the classical signal processing approaches such as wavelets, non-local processing, compressed sensing, etc, is still not well understood. To address these issues, here we show that the long-searched-for missing link is the convolutional framelets for representing a signal by convolving local and non-local bases. The convolutional framelets was originally developed to generalize the theory of low-rank Hankel matrix approaches for inverse problems, and this paper significantly extends the idea to derive a deep neural network using multi-layer convolutional framelets with perfect reconstruction (PR) under rectified linear unit (ReLU) nonlinearity. Our analysis also shows that the popular deep network components such as residual block, redundant filter channels, and concatenated ReLU (CReLU) indeed help to achieve the PR, while the pooling and unpooling layers should be augmented with multi-resolution convolutional framelets to achieve PR condition. This discovery reveals the limitations of many existing deep learning architectures for inverse problems, and leads us to propose a novel *deep convolutional framelets* neural network. Using numerical experiments with sparse view x-ray computed tomography (CT), we demonstrated that our deep convolution framelets network shows consistent improvement over existing deep architectures at all downsampling factors. This discovery suggests that the success of deep learning is not from a magical power of a black-box, but rather comes from the power of a novel signal representation using non-local basis combined with data-driven local basis, which is indeed a natural extension of classical signal processing theory.

Index Terms

Convolutional framelets, deep learning, inverse problems, ReLU, perfect reconstruction condition

Correspondence to:

Jong Chul Ye, Ph.D

KAIST Endowed Chair Professor

Department of Bio and Brain Engineering

Department of Mathematical Sciences

Korea Advanced Institute of Science and Technology (KAIST)

291 Daehak-ro, Yuseong-gu, Daejeon 34141, Republic of Korea

Tel: +82-42-350-4320

Email: jong.ye@kaist.ac.kr

I. INTRODUCTION

DEEP learning approaches have achieved tremendous success in classification problems [1] as well as low-level computer vision problems such as segmentation [2], denoising [3], super resolution [4], [5], etc. The theoretical origin of its success has been investigated [6], [7], and the exponential expressivity under a given network complexity (in terms of VC dimension [8] or Rademacher complexity [9]) has been often attributed to its success. A deep network is also known to learn high-level abstractions/features of the data similar to the visual processing in human brain using multiple layers of neurons with non-linearity [10].

Inspired by the success of deep learning in low-level computer vision, several machine learning approaches have been recently proposed for image reconstruction problems. In X-ray computed tomography (CT), Kang et al [11] provided the first systematic study of deep convolutional neural network (CNN) for low-dose CT and showed that a deep CNN using directional wavelets is more efficient in removing low-dose related CT noises. Unlike these low-dose artifacts from reduced tube currents, the streaking artifacts originated from sparse projection views show globalized artifacts that are difficult to remove using conventional denoising CNNs [12], [13]. Jin et al [14] and Han et al [15] independently proposed a residual learning using U-Net [2] to remove the global streaking artifacts caused by sparse projection views. In MRI, Wang et al [16] was the first to apply deep learning to compressed sensing MRI (CS-MRI). They trained the deep neural network from the downsampled reconstruction images to learn a fully sampled reconstruction. Then, they used the deep learning result either as an initialization or as a regularization term in classical CS approaches. Deep network architecture using unfolded iterative CS algorithm was also proposed [17]. Instead of using handcrafted regularizers, the authors in [17] tried to learn a set of optimal regularizers. Multilayer perceptron was developed for accelerated parallel MRI [18]. Domain adaptation from sparse view CT network to projection reconstruction MRI was also proposed [19]. These pioneering works consistently showed impressive reconstruction performances, which are often superior to the existing iterative approaches.

However, the more we have observed impressive empirical results in image reconstruction problems, the more unanswered questions we encounter. For example, to our best knowledge, we do not have the answers to the following questions that are critical to a network design:

- 1) What is the role of the nonlinearity such as rectified linear unit (ReLU) ?
- 2) What is the role of the filter channels in convolutional layers ?
- 3) Why do we need a pooling and unpooling in some architectures ?
- 4) Why do some networks need a fully connected layers whereas the others do not ?
- 5) What is the role of by-pass connection or residual network ?

Furthermore, the most troubling issue for signal processing community is that we do not know clearly

why it works, and the link to the classical signal processing theory is still not clearly understood. For example, wavelets [20] has been extensively investigated as an efficient signal representation theory for many image processing applications by exploiting energy compaction property of the expansion. Compressed sensing theory [21], [22] has further extended the idea to demonstrate that an accurate recovery is possible from undersampled data, if the signal is sparse in some frames and the sensing matrix is incoherent. Non-local image processing techniques such as non-local means [23], BM3D [24], etc have also demonstrated impressive performance for many image processing applications. The link between these algorithms have been extensively studied for last few years using various mathematical tools from harmonic analysis, convex optimization, etc. However, recent years have witnessed that a blind application of deep learning toolboxes sometimes provides even better performance than mathematics-driven classical signal processing approaches. Does this imply the dark age of signal processing or a new opportunity ?

Therefore, the main goal of this paper is to address these open questions. In fact, our paper is not the only attempt to address these issues. For example, the interpretation of a deep network in terms of unfolded (or unrolled) sparse recovery has been one of the prevailing views in research community [14], [17], [25], [26]. However, this interpretation still does not give an answer to several key questions: for example, why do we need multichannel filters ? In this paper, we therefore depart from this existing view and propose a new interpretation of a deep network as a novel *signal representation* scheme. In fact, signal representation theory such as wavelets and frames have been active areas of researches in many years [27], and Bruna et al [28] recently proposed a wavelet scattering network as a translation invariant image representation. However, this approach does not have learning components as in the existing deep learning networks.

Then, what is missing here? One of the most important contributions of our work is to show that the geometry of deep learning can be revealed by *lifting* a signal to a high dimensional space using Hankel structured matrix. More specifically, the lifted Hankel structure matrix can be factorized into non-local, and local basis matrices as well as positive sparse matrix that has energy compaction property. This leads to a frame representation of signals using two bases: non-local and local bases. Our novel discovery is the realization that the non-local basis determines the network architecture such as pooling/unpooling, whereas the local basis enables the network to learn convolution filters. More specifically, for a given nonlocal basis, the local basis is trained such that it provides the maximal energy compaction of true signals while the noise and artifacts can be spread out. In other words, the application specific knowledge guides us to a better choice of a fixed non-local basis, on which the local basis are learned to maximize the performance.

We demonstrate that the power of deep learning indeed comes from the optimal interplay between the nonlocal and local bases. In fact, the idea of exploiting the two bases by the convolutional framelets was

originally proposed by Yin et [29]. However, the aforementioned close link to the deep neural network was not revealed in [29]. Most importantly, we demonstrate for the first time the importance of the perfect reconstruction (PR) condition under rectified linear unit (ReLU). Furthermore, the mysterious role of the redundant multichannel filters and residual network can be easily understood as important tools to satisfy the PR condition under ReLU. In particular, by augmenting local filters with paired filters with opposite phase, the ReLU nonlinearity disappears and the deep convolutional framelet becomes a linear signal representation. However, to make the deep network linear, the number of channels should increase exponentially along the layer, which is not practical. In the case when the number of filter channel are not sufficient, we show that the deep convolutional framelet is equivalent to the low-rank approximation of Hankel matrix. Finally, to overcome the limitation of the pooling and unpooling layers, we derive a multi-resolution analysis (MRA) for convolutional framelets using wavelet-based non-local basis.

Seeing with the new eyes of deep convolutional framelets, we analyze the limitations of the existing deep learning architecture for inverse problems. Accordingly, we propose a new class of deep learning network which results in consistent performance improvement over the existing deep learning approaches. We call the new class of deep network using convolutional framelets as the *deep convolutional framelets*.

A. Notations

For a matrix A , $R(A)$ denotes the range space of A and $N(A)$ refers to the null space of A . $P_{R(A)}$ denotes the projection to the range space of A , whereas $P_{R(A)}^\perp$ denotes the projection to the orthogonal complement of $R(A)$. The notation $0_{p \times q}$ means the $p \times q$ zero matrix. The $n \times n$ identity matrix is referred to as $I_{n \times n}$. For a given matrix $A \in \mathbb{R}^{m \times n}$, the notation A^\dagger refers to the generalized inverse. The superscript $^\top$ of A^\top denotes the Hermitian transpose. Because we are mainly interested in real valued cases, $^\top$ is equivalent to the transpose T . The inner product in matrix space is defined by $\langle A, B \rangle = \text{Tr}(A^\top B)$, where $A, B \in \mathbb{R}^{n \times m}$. For a matrix A , $\|A\|_F$ denotes its Frobenius norm.

II. LOW-RANK HANKEL MATRIX APPROACHES

In this section, we review the theory of annihilating filter-based low-rank Hankel matrix approach (ALOHA) [30]–[36], which have been recently proposed as powerful image processing and inverse problem techniques. For simplicity, our theory is developed using 1-D signal model, but the extension to multi-dimensional signal model is straightforward. We first begin with some mathematical preliminaries.

A. Hankel Matrix

A (wrap-around) Hankel matrix can be easily obtained from (circular) convolution [30]. In this paper, to avoid special treatment of boundary condition, our theory is mainly derived using circular convolution.

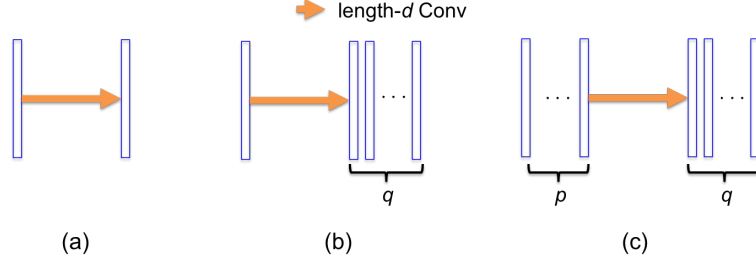


Fig. 1. Convolutional operations in CNN and their Hankel matrix representations. (a) Single-input single-output convolution $y = \mathbb{H}_d(f)h$, (b) single-input multi-output convolution $Y = \mathbb{H}_d(f)H$ and (c) multi-input multi-output convolution $Y = \mathbb{H}_{d|p}(f)H$.

More specifically, let $f = [f[1], \dots, f[n]]^T \in \mathbb{R}^n$ and $h = [h[1], \dots, h[d]]^T \in \mathbb{R}^d$ be an input image and a convolutional filter kernel. Then, a single-input single-output convolution $y = h \otimes f$ can be represented in a matrix form:

$$y = \mathbb{H}_d(f)h,$$

where $\mathbb{H}_d(f)$ is a wrap-around Hankel matrix

$$\mathbb{H}_d(f) = \begin{bmatrix} f[1] & f[2] & \cdots & f[d] \\ f[2] & f[3] & \cdots & f[d+1] \\ \vdots & \vdots & \ddots & \vdots \\ f[n-d+1] & f[n-d+2] & \cdots & f[n] \\ f[n-d+2] & f[n-d+3] & \cdots & f[1] \\ \vdots & \vdots & \ddots & \vdots \\ f[n] & f[1] & \cdots & f[d-1] \end{bmatrix}. \quad (1)$$

Similarly, a single-input multi-output (SIMO) convolution using d -length filters $h_1, \dots, h_q \in \mathbb{R}^d$ can be represented by

$$Y = \mathbb{H}_d(f)H \quad (2)$$

where

$$Y := [y_1 \ \cdots \ y_q] \in \mathbb{R}^{n \times q}, \quad H := [h_1 \ \cdots \ h_q] \in \mathbb{R}^{d \times q}, \quad (3)$$

and q denotes the number of output channels. On the other hand, multi-input multi-output (MIMO) convolution can be represented by

$$y_i = \sum_{j=1}^p f_j \otimes h_i^j, \quad i = 1, \dots, q \quad (4)$$

where p and q are the number of input and output channels, respectively; $h_i^j \in \mathbb{R}^d, i = 1, \dots, q; j = 1, \dots, p$ refer to the corresponding filters with the filter length d . The corresponding matrix representation is then

given by

$$Y = \sum_{j=1}^p \mathbb{H}_d(f_j) H^j = \mathbb{H}_{d|p}([f_1 \cdots f_p]) \begin{bmatrix} H^1 \\ \vdots \\ H^p \end{bmatrix} \quad (5)$$

where $\mathbb{H}_{d|p}([f_1 \cdots f_p])$ is an *extended Hankel matrix* by stacking p -Hankel matrix side by side:

$$\mathbb{H}_{d|p}([f_1 \cdots f_p]) := [\mathbb{H}_d(f_1) \quad \mathbb{H}_d(f_2) \quad \cdots \quad \mathbb{H}_d(f_p)] \quad (6)$$

and

$$Y = [y_1 \quad \cdots \quad y_q] \in \mathbb{R}^{n \times q}, \quad H^j = [h_1^j \quad \cdots \quad h_q^j] \in \mathbb{R}^{d \times q}.$$

For notational simplicity, we denote $\mathbb{H}_{d|1}([f]) = \mathbb{H}_d(f)$. Note that the aforementioned matrix vector operations are equivalent to the filtering operation used in the existing convolutional neural networks (CNN) [1] as shown in Fig. 1(a)-(c).

We denote the space of the wrap-around Hankel structure matrices of the form in (1) as $\mathcal{H}(n, d)$ and an extended Hankel matrix with p -Hankel matrix of the form in (6) as $\mathcal{H}(n, d; p)$. The following element calculus in $\mathcal{H}(n, d)$ and $\mathcal{H}(n, d; p)$ (some are obtained from [30] and [29]) are useful.

Lemma 2.1. *Let the space of wrap-around Hankel matrix $\mathcal{H}(n, d)$ be equipped with the matrix inner product $\langle A, B \rangle = \text{Tr}(A^\top B)$. For $k = 1, \dots, n$, define*

$$A_k = \frac{1}{\sqrt{d}} \mathbb{H}_d(e_k) \in \mathcal{H}(n, d) \quad (7)$$

where e_k denotes the standard coordinate vector in \mathbb{R}^n with only k -th element as one. Then, the following statements are true.

- 1) The set $\{A_k\}_{k=1}^n$ is the orthonormal basis for the space of $\mathcal{H}(n, d)$.
- 2) For a given $f \in \mathbb{R}^n$ and the associated Hankel matrix $\mathbb{H}_d(f) \in \mathcal{H}(n, d)$, we have

$$F := \mathbb{H}_d(f) = \sum_{k=1}^n \langle A_k, F \rangle A_k \quad \text{where} \quad \langle A_k, \mathbb{H}_d(f) \rangle = \sqrt{d} f[k]. \quad (8)$$

- 3) Let $u \in \mathbb{R}^n$ and $v \in \mathbb{R}^d$. Then, for any Hankel matrix $F = \mathbb{H}_d(f) \in \mathcal{H}(n, d)$, we have

$$\langle F, uv^\top \rangle = u^\top F v = u^\top (f \otimes v) = f^\top (u \otimes v) = \langle f, u \otimes v \rangle \quad (9)$$

where \otimes denotes the circular convolution.

- 4) For a given A_k in (7) and any $u \in \mathbb{R}^n$ and $v \in \mathbb{R}^d$,

$$\langle A_k, uv^\top \rangle = \frac{1}{\sqrt{d}} (u \otimes v)[k]. \quad (10)$$

5) A generalized inverse of the lifting (8) is given by

$$\mathbb{H}_d^\dagger(B) = \frac{1}{\sqrt{d}} \begin{bmatrix} \langle A_1, B \rangle \\ \langle A_2, B \rangle \\ \vdots \\ \langle A_n, B \rangle \end{bmatrix} \quad (11)$$

where B is any matrix in $\mathbb{R}^{n \times d}$.

6) For $\Phi \in \mathbb{R}^{n \times n}$ and $C \in \mathbb{R}^{n \times q}$ and $\tilde{\Psi} \in \mathbb{R}^{d \times q}$,

$$\mathbb{H}_d^\dagger(\Phi C \tilde{\Psi}^\top) = \sum_{i=1}^q \mathbb{H}_d^\dagger(\Phi c_i \tilde{\psi}_i^\top) = \frac{1}{q} \sum_{i=1}^q ((\Phi c_i) \otimes \tilde{\psi}_i) \in \mathbb{R}^n. \quad (12)$$

7) Let $\mathbb{H}_{d|p}^\dagger(\cdot)$ denote the generalized inverse of an extended Hankel operator $\mathbb{H}_{d|p}(\cdot)$. Suppose, furthermore, $C = [C_1 \ \dots \ C_p] \in \mathbb{R}^{n \times dp}$ with $C_i \in \mathbb{R}^{n \times d}$, $i = 1, \dots, p$. Then, we have

$$\mathbb{H}_{d|p}^\dagger(C) = [\mathbb{H}_d^\dagger(C_1) \ \dots \ \mathbb{H}_d^\dagger(C_p)] \in \mathbb{R}^{n \times p} \quad (13)$$

Proof. See Appendix. □

B. Low-rank Hankel Structured Matrix Approaches for Inverse Problems

Hankel matrix has arisen repeatedly from many different contexts in signal processing and control theory. In control theory, the low rank Hankel matrix has been used in system identification [37]. In signal processing theory, Hankel matrix has been widely used for harmonic retrieval and array signal processing [38], subspace-based channel identification [39], just to name a few. Recent advance in this field [30] is the discovery that a low-rank Hankel matrix is closely linked to the sampling theory of signals with the finite rate of innovations (FRI) [40]. More specifically, the rank of the Hankel matrix is directly related to the length of the annihilating filter as shown in the following theorem:

Theorem 2.2. [30] Let $r + 1$ denote the minimum length of annihilating filters that annihilates data $f = [f[1], \dots, f[n]]^T$. Then, for a given Hankel structured matrix $\mathbb{H}_d(f) \in \mathcal{H}(n, d)$ whose number of columns and rows are bigger than r , we have

$$\text{RANK}\mathbb{H}_d(f) = r, \quad (14)$$

where $\text{RANK}(\cdot)$ denotes a matrix rank.

Here, the annihilating filter h , which is the key component of FRI sampling theory [40], is defined as the filter satisfying

$$f \otimes h = \mathbb{H}_d(f)h = 0. \quad (15)$$

Vetterli et al [40] derived the explicit forms of the minimum length annihilating filters for FRI signals, which shows that the minimum annihilating filter length is directly related to the rate of innovation or the

sparsity level of the original signal in the reciprocal domain [40]. Therefore, the rank of the Hankel matrix is determined by the sparsity level in the signal in the reciprocal domain [30]. Furthermore, we provided the necessary and sufficient condition for a Hankel matrix to have low rank property, which showed that a generalized form of FRI signals with (damped) exponentials is the only signal class that has low rank Hankel matrix in the reciprocal domain [30]. In [32], we also showed the rank of the extended Hankel matrix in (6) can be further reduced when the multiple signals f_1, \dots, f_p share the same support in the reciprocal domain or have the joint sparsity [32].

The low-rank Hankel matrix is very useful in many inverse problem as demonstrated by many applications [31]–[36]. For example, if the Fourier data is sparsely sampled, the missing Fourier data can be interpolated by lifting the Fourier data into a Hankel structure matrix and applying the low-rank matrix completion algorithms [32]–[35]. In these applications, the low-rank Hankel matrix is constructed in the Fourier domain; however, the dual construction of low-rank Hankel matrix in the image domain is possible. More specifically, in [31] we showed that when an image is partitioned into smooth, edged or textured patches, the corresponding spectrum is sparse; thus, the lifted Hankel matrix can be constructed in the image domain to reveal the low rank structure. This idea can be used for image denoising [41], artifact removal [36] and deconvolution [42], by modeling the underlying intact signals to have low-rank Hankel structure, from which the artifacts or blur components can be easily removed. Moreover, the joint sparsity was exploited using extended Hankel matrix for parallel MRI [32], MR echo planar imaging (EPI) ghost artifact correction [35], etc. However, the main disadvantages of these low rank Hankel matrix approach is the computational complexity due to the matrix factorization in each iterative step.

Note that the low-rank Hankel matrix algorithms usually assume the form of patch-by-patch processing in the low level computer vision problems such as denosing [41] or inpainting [31], whereas the global k-space data processing is used for MR applications [32]–[35]. It is also interesting to note that this is similar to the current practice of deep network for image reconstruction and low level computer vision applications, where the image domain approach is usually done in patch-based processing, while the whole k-space processing is often used for deep learning MR reconstruction [17]. Later, we will show that this is not a coincident; rather it suggests an important connection of low-rank Hankel matrix approach to deep learning.

III. CONVOLUTIONAL FRAMELETS AND ITS EXTENSION

In this section, we review the theory of convolutional framelets [29], and discuss our novel extensions.

A. *Review*

The convolutional framelets by Yin et al [29] is a novel signal representation scheme combining the local and nonlocal characterization of patches in an image. The representation scheme was shown to be equivalent

to a tight frame constructed from convolving local basis with nonlocal basis. Specifically, the image patch is first lifted to a form of Hankel matrix, from which nonlocal and local bases are obtained. This results in sparse expansion coefficients if the underlying Hankel matrix has low dimensional structure [29].

Specifically, for a given n -dimensional vector $f \in \mathbb{R}^n$, let the image patch lifted to Hankel structured matrix be denoted by $F := \mathbb{H}_d(f) \in \mathcal{H}(n, d)$. Suppose, furthermore, that Φ and Ψ denote the two orthonormal matrices of dimension $n \times n$ and $d \times d$, respectively, denoting the columns of Φ and Ψ as ϕ_i and ψ_j , respectively. Then, Yin et al showed the following result [29]:

Proposition 3.3 ([29]). *Let ϕ_i and ψ_j denotes the i -th and j -th columns of orthonormal matrix $\Phi \in \mathbb{R}^{n \times n}$ and $\Psi \in \mathbb{R}^{d \times d}$, respectively. Then, for any n -dimensional vector $f \in \mathbb{R}^n$, we have*

$$f = \frac{1}{d} \sum_{i=1}^n \sum_{j=1}^d \langle f, \phi_i \otimes \psi_j \rangle \phi_i \otimes \psi_j \quad (16)$$

Furthermore, $\phi_i \otimes \psi_j$ with $i = 1, \dots, n; j = 1, \dots, d$ form a tight frame for \mathbb{R}^n with the frame constant d .

Yin et al argued that the convolution frame $\phi_i \otimes \psi_j$ has both local and non-local properties, claiming that $\{\psi_j\}_{j=1}^d$ forms either local or non-local basis whereas $\{\phi_i\}_{i=1}^n$ forms the other [29]. They further maintained that the superior energy compaction property emerges when the two bases are chosen to exploit the low-dimensional structure of Hankel matrix [29]. By energy compaction, it is implied that there are only a few non-zero values for the expansion coefficients or at least most of the energy is concentrated in only a few expansion coefficients. Specifically, Yin et al [29] solves the following optimization problem for a given orthonormal basis Φ :

$$\max_{\Psi \in \mathbb{R}^{d \times d}} \sum_{1 \leq i \leq j \leq r} C_{ij}^2 \quad , \quad \text{subject to } C = \Phi^\top F \Psi, \quad \Psi^\top \Psi = I_{d \times d} \quad (17)$$

which maximizes the elements in the upper triangular part of upper $r \times r$ block. Thus, the design criterion by Yin et al [29] attempts to maximize energy concentration in this region, and the degree of energy concentration is again determined by the rank r of Hankel matrix.

B. Extensions

While the original convolutional framelets by Yin et al [29] exploits the advantages of the low rank Hankel matrix approaches using two bases, there are several limitations. Specifically, their convolutional framework uses only orthonormal basis. More importantly, the significance of multi-layer implementation using convolutional framelets was not noticed. In this section, we show that these limitations can be readily addressed if the original problem is lifted to a high-dimensional optimization problem using Hankel matrix. Later, we will show that the resulting high dimensional problem is directly linked to a neural network when it is combined with nonlinearity.

Proposition 3.4. Let ϕ_i and ψ_j denotes the i -th and the j -th columns of matrix $\Phi \in \mathbb{R}^{n \times m}$ and $\Psi \in \mathbb{R}^{d \times q}$, respectively. Then, for any n -dimensional vector $f \in \mathbb{R}^n$, under the following resolution of identities,

$$\tilde{\Phi}\Phi^\top = \sum_{i=1}^m \tilde{\phi}_i \phi_i^\top = I_{n \times n}, \quad (18)$$

$$\tilde{\Psi}\Psi^\top = \sum_{j=1}^q \tilde{\psi}_j \psi_j^\top = I_{d \times d}, \quad (19)$$

we have

$$f = \frac{1}{d} \sum_{i=1}^m \sum_{j=1}^q \langle f, \phi_i \otimes \psi_j \rangle \tilde{\phi}_i \otimes \tilde{\psi}_j. \quad (20)$$

Proof. Let $F := \mathbb{H}^d(f)$. Then, using the resolution of identity (18) and (19), we have

$$\begin{aligned} F &= \tilde{\Phi}\Phi^\top F \tilde{\Psi}\Psi^\top \\ &= \sum_{i=1}^m \sum_{j=1}^q \tilde{\phi}_i \phi_i^\top F \psi_j \tilde{\psi}_j^\top \\ &= \sum_{i=1}^m \sum_{j=1}^q \langle \Psi_{ij}, F \rangle \tilde{\Psi}_{ij} \end{aligned}$$

where $\Psi_{ij} := \phi_i \psi_j^\top$ and $\tilde{\Psi}_{ij} = \tilde{\phi}_i \tilde{\psi}_j^\top$ and we use the following identity:

$$\phi_i^\top F \psi_j = \text{Tr}(\Psi_{ij}^\top F) = \langle \Psi_{ij}, F \rangle$$

Moreover, using (9), we have

$$\phi_i^\top F \psi_j = \langle f, \phi_i \otimes \psi_j \rangle.$$

and using (11) and (10), we have

$$\mathbb{H}_d^\dagger(\tilde{\phi}_i \tilde{\psi}_j^\top) = \frac{1}{d} \begin{bmatrix} (\tilde{\phi}_i \otimes \tilde{\psi}_j)[1] \\ \vdots \\ (\tilde{\phi}_i \otimes \tilde{\psi}_j)[n] \end{bmatrix} = \frac{1}{d} \tilde{\phi}_i \otimes \tilde{\psi}_j$$

Therefore, we have

$$f = \mathbb{H}_d^\dagger(F) = \frac{1}{d} \sum_{i=1}^m \sum_{j=1}^q \langle f, \phi_i \otimes \psi_j \rangle \tilde{\phi}_i \otimes \tilde{\psi}_j$$

Q.E.D. □

Remark 3.5. Here, the column of the local basis Ψ and $\tilde{\Psi}$ are often referred to as local filters and its dual filters. In addition, we often call Φ^\top as non-local transform because it transform the filtered signals by multiplying Φ^\top . If the nonlocal basis Φ is orthonormal, then Φ corresponds to the inverse non-local transform.

Note that the perfect recovery condition (20) can be equivalently studied using:

$$f = \mathbb{H}_d^\dagger(\tilde{\Phi}(\Phi^\top \mathbb{H}_d(f) \Psi) \tilde{\Psi}^\top). \quad (21)$$

In general, for a given matrix input $Z \in \mathbb{R}^{n \times p}$, the perfect reconstruction condition for matrix Z can be given

by

$$Z = \mathbb{H}_{d|p}^\dagger (\tilde{\Phi}(\Phi^\top \mathbb{H}_{d|p}(Z) \Psi) \tilde{\Psi}^\top) . \quad (22)$$

C. Examples

1) *Pooling and Unpooling*: So far, we have claimed that the non-local basis $\Phi \in \mathbb{R}^{n \times m}$ is required to satisfy (18) for the PR condition. However, there are some popular non-local transform structures that do not satisfy the requirement. For example, pooling and unpooling layers in the deep neural network corresponds to a non-local transform that convert signals to a different resolution. These are quite often used in classifier design as well as segmentation network [43]. Specifically, the average and max pooling operators $\Phi_{ave}, \Phi_{max} \in \mathbb{R}^{n \times \frac{n}{2}}$ for $f \in \mathbb{R}^n$ is defined as follows:

$$\Phi_{ave} = \frac{1}{\sqrt{2}} \begin{bmatrix} 1 & 0 & \cdots & 0 \\ 1 & 0 & \cdots & 0 \\ 0 & 1 & \cdots & 0 \\ 0 & 1 & \cdots & 0 \\ \vdots & \vdots & \ddots & \vdots \\ 0 & 0 & \cdots & 1 \\ 0 & 0 & \vdots & 1 \end{bmatrix}, \quad \Phi_{max} = \begin{bmatrix} b_1 & 0 & \cdots & 0 \\ 1 - b_1 & 0 & \cdots & 0 \\ 0 & b_2 & \cdots & 0 \\ 0 & 1 - b_2 & \cdots & 0 \\ \vdots & \vdots & \ddots & \vdots \\ 0 & 0 & \cdots & b_{\frac{n}{2}} \\ 0 & 0 & \vdots & 1 - b_{\frac{n}{2}} \end{bmatrix} \quad (23)$$

where $\{b_i\}_i$ in max pooling are random $(0, 1)$ binary numbers that are determined by the signal statistics. We can easily see that the columns of max pooling or average pooling are orthonormal to each other; however, it does not constitute a basis because it does not span \mathbb{R}^n . Then, what does this network perform?

Recall that the standard unpooling layer $\tilde{\Phi}$ has the same form of the pooling, i.e. $\tilde{\Phi} = \Phi$. In this case, under the biorthogonality condition for the local filters, i.e. $\Psi \tilde{\Psi}^\top = I_{d \times d}$, the signal after pooling and unpooling becomes:

$$\hat{f} = \mathbb{H}_d^\dagger (\Phi(\Phi^\top \mathbb{H}_d(f)) = \Phi \Phi^\top f$$

which is basically a low-pass filtered signal. This works fine for the segmentation problem; but, a care needs to be taken for the case of image restoration, because the goal is to keep the details of the signal. In fact, this limitation of pooling and unpooling can be easily addressed by the multi-resolution analysis of convolutional framelets, which is the main topic of the next section.

2) *Spectral Basis*: Unlike the pooling and unpooling, the spectral basis still guarantees the perfect reconstruction even though the corresponding local or non-local transforms perform dimension reduction. More specifically, suppose that the Hankel matrix $F := \mathbb{H}_d(f) \in \mathcal{H}(n, d)$ with rank $r < d$ have the following singular value decomposition:

$$F = U \Sigma V^\top$$

where $U \in \mathbb{R}^{n \times r}$ and $V \in \mathbb{R}^{d \times r}$ denote the left and right singular vector bases, and $\Sigma \in \mathbb{R}^{r \times r}$ is the diagonal matrix whose diagonal components contains the singular values. Then, we can easily show that Proposition 3.4 can still hold even with nonlocal and local basis $\Phi, \tilde{\Phi} \in \mathbb{R}^{n \times m}$ and $\Psi, \tilde{\Psi} \in \mathbb{R}^{d \times q}$ with $m < n$ and $q < d$ satisfying

$$\tilde{\Phi}\Phi^\top = \sum_{i=1}^m \tilde{\phi}_i \phi_i^\top = P_{R(U)} \quad (24)$$

$$\tilde{\Psi}\Psi^\top = \sum_{j=1}^q \tilde{\psi}_j \psi_j^\top = P_{R(V)}. \quad (25)$$

This is because

$$F = P_{R(U)} F P_{R(V)}.$$

However, the corresponding $\tilde{\Phi}$ is usually a dense matrix dependent on the specific input signal. A data-dependent dense structure of unpooling matrix is prohibited due to its huge memory requirement. For example, if one is interested in processing 512×512 (i.e. $n = 2^9 \times 2^9$) image using dense form of pooling/unpooling matrices, the required memory becomes 2^{37} , which is not possible to store or estimate.

D. Perfect Reconstruction and Inverse Problems

So far, we have investigated the perfect recovery (PR) condition for convolutional framelets and we are now ready to explain why the perfect recovery condition is important. This is because the PR is usually associated with the energy compact property [27].

Consider an inverse problem to obtain the noiseless signal $f \in \mathbb{R}^n$ from a noisy measurement $g \in \mathbb{R}^n$ through a sensing matrix \mathcal{A} :

$$g = \mathcal{A}f + e,$$

where $e \in \mathbb{R}^n$ is the noise. Suppose that we have an nonlocal transform $\Phi^{(0)\top}$ that approximates a generalized inverse of the sensing matrix. Then, the application of the nonlocal transform leads to

$$y := \Phi^{(0)\top} g = f + \underbrace{\Phi^{(0)\top} e + (\Phi^{(0)\top} \mathcal{A} - 1)f}_w$$

where w is considered as an artifact component. Because the noise is additive, if the measurement is lifted to a Hankel structured matrix, we have

$$Y = F + W$$

where $Y, F, W \in \mathcal{H}(n, d)$ are lifted wrap-around Hankel matrices from y, f and w , respectively. Now, the lifted Hankel matrix reveals important geometry. More specifically, F matrix from the noiseless signal is low-ranked as shown by the theory of low-rank Hankel matrix approach [30], whereas W is usually full-ranked because the noise does not have any low dimensional structure. Indeed, this observation has been

successfully used in the annihilating filter-based low rank Hankel matrix approaches for image denoising [41], artifact removal [36] and deconvolution [42].

Thus, if we choose the nonlocal and local bases to have energy compaction, the most dominant convolutional framelet coefficients are from the underlying intact signals, so we can apply some operations to remove the remaining framelet coefficients and to obtain the noise reduced image. In the classical signal representation approaches such as wavelets, this is usually done using shrinkage operation such as soft-thresholding [44]. However, in the following section, we will show that there is a better way, which is directly related to neural network learning.

IV. DEEP CONVOLUTIONAL FRAMELETS NEURAL NETWORKS

In this section, we will show that the convolutional framelets is directly related to the deep neural network when combined with multilayer implementation and nonlinearity. Moreover, our convolutional framelets can explain additional components of deep learning: redundant convolutional filters and advanced network components such as residual block [47]. Amazingly, the ReLU nonlinearity plays the key important role in this analysis.

A. From Convolutional Framelets to Neural Network

Note that the convolutional framelet expansion (22) can be written as follows:

$$Z = \mathbb{H}_{d|p}^\dagger (\tilde{\Phi} C \tilde{\Psi}^\top), \quad (\text{decoder step}) \quad (26)$$

$$C = \Phi^\top \mathbb{H}_{d|p}(Z) \Psi \quad (\text{encoder step}) \quad (27)$$

where we interpret each step as decoder or encoder step. Thanks to the Hankel matrix representation of convolution in (2), it is easy to see that the encoder step corresponds to the MIMO convolution followed by a non-local transform. On the other hand, the decoder step in (26) appears complicated due to the existence of the inverse Hankel operation $\mathbb{H}_{d|p}^\dagger$. Amazingly, we can show that this operation is indeed equivalent to the decoder step in standard CNN, which composed of global transform followed by channel-wise filtering using $\{h_i\}$ and inter-channel weighting operation with R (see Fig. 2(a)). This is formally proven by the following proposition:

Proposition 4.6. *Fig. 2(b) is a realization of $\mathbb{H}_{d|p}^\dagger (\Phi \hat{C} \tilde{\Psi}^\top)$ where $\Phi \in \mathbb{R}^n$ and $\tilde{\Psi} \in \mathbb{R}^{pd \times pd}$. Furthermore, there exists a filter set $\{\tilde{\psi}_{i,j}\}$ such that Fig. 2(a) and Fig. 2(b) are equivalent.*

Proof. Let

$$\tilde{\Psi}^\top = [\tilde{\Psi}_1^\top \dots \tilde{\Psi}_p^\top], \quad \text{where} \quad \tilde{\Psi}_j^\top \in \mathbb{R}^{pd \times d}$$

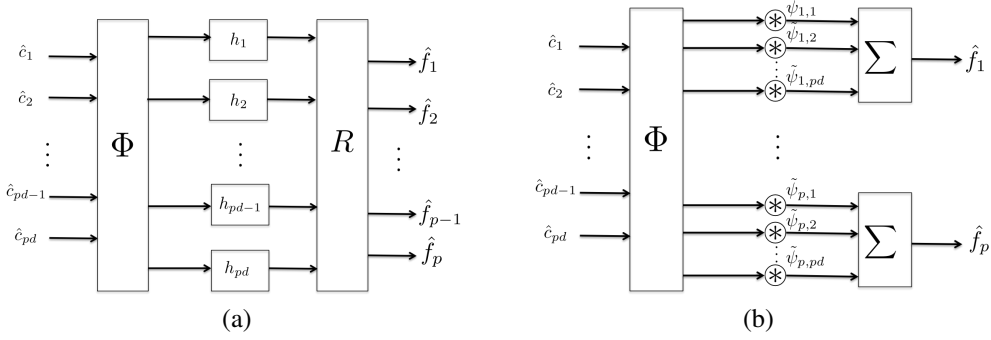


Fig. 2. Equivalence of decoder part of CNN and convolutional framelet. (a) CNN, and (b) convolutional framelet.

Thus,

$$\Phi \hat{C} \tilde{\Psi}^\top = [\Phi \hat{C} \tilde{\Psi}_1^\top \quad \dots \quad \Phi \hat{C} \tilde{\Psi}_p^\top].$$

Using (12) and (13), we have

$$\begin{aligned} \mathbb{H}_{d|p}^\dagger (\Phi \hat{C} \tilde{\Psi}^\top) &= [\mathbb{H}_d^\dagger (\Phi \hat{C} \tilde{\Psi}_1^\top) \quad \dots \quad \mathbb{H}_d^\dagger (\Phi \hat{C} \tilde{\Psi}_{p(l)}^\top)] \\ &= \frac{1}{pd} [\sum_{i=1}^{pd} ((\Phi \hat{c}_i) \otimes \tilde{\psi}_{1,i}) \quad \dots \quad \sum_{i=1}^{pd} ((\Phi \hat{c}_i) \otimes \tilde{\psi}_{p,i})] \end{aligned}$$

where $\tilde{\psi}_{j,i}$ denotes the i -th column of $\tilde{\Psi}_j$. This implies that \hat{c}_i should be first transformed with the nonlocal transform Φ to obtain $\Phi \hat{c}_i$, which is then filtered with the pd number of biorthogonal filters $\{\tilde{\psi}_{j,i}\}_j$. Then, the final output should be given as the sum of these filtered signals for each block. Next, we will show the equivalence between Fig. 2(a) and (b). The operation in Fig. 2(a) can be mathematically represented by

$$f_j = \sum_{i=1}^{pd} r_{ij} (\Phi \hat{c}_i \otimes h_i), \quad j = 1, \dots, p$$

where $\{h_i\}_{i=1}^{pd}$ corresponds to the filters within channel and $R = [r_{ij}]_{i,j=1}^{pd,p}$ denotes the inter-channel weighting matrix. Therefore, by choosing the local filter as follows:

$$\tilde{\psi}_{j,i} = pd r_{ij} h_i, \quad i = 1, \dots, pd, \quad j = 1, \dots, p$$

we can make Fig. 2(a) and (b) equivalent. Q.E.D. □

Thus, the decoder step is equivalent to a standard CNN layer composed of global transform followed by channel-wise filtering using and inter-channel weighting operation with 1×1 filters as illustrated by the blue line in Fig. 3(a). The associated encoder step is then the analysis part of convolutional framelets that computes the framelet coefficients $\Phi^\top \mathbb{H}_{d|p}(f) \Psi$ (see red line in Fig. 3(a)). This suggests that the convolutional framelets is closely related to deep learning if multiple convolutional framelet expansions are cascaded sequentially while retaining the encoder-decoder architecture (see Fig. 3(b)). The low rank

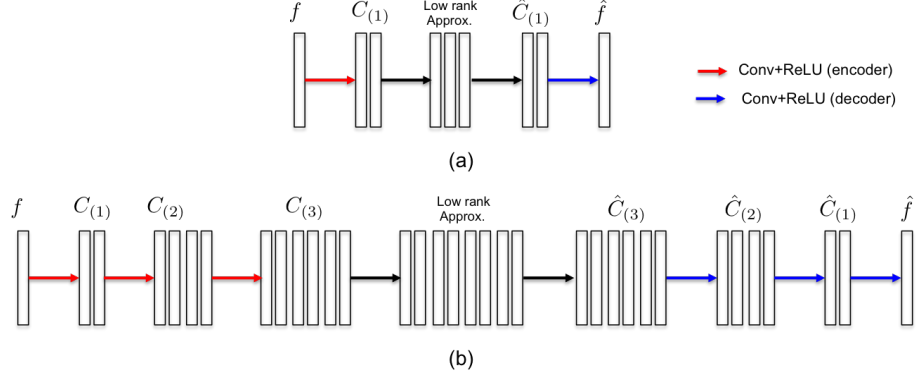


Fig. 3. (a) One layer encoder-decoder, and (b) multi-layer encoder-decoder architectures.

approximation part of Fig. 3(a)(b) will be explained later.

In order to reveal a more closer link between the convolutional framelets and the deep network, we further need to consider the nonlinearity and the multi-layer implementation. Note that the ReLU nonlinearity [45], [46] is currently most widely used for deep learning approaches. Specifically, the ReLU $\rho(\cdot)$ is an element-wise operation for a matrix such that for a matrix $A = [a_{ij}]_{i,j=1}^{n,m} \in \mathbb{R}^{n \times m}$, the ReLU operator provides non-negative part, i.e. $\rho(A) = [\max(0, a_{ij})]_{i,j=1}^{n,m}$. To incorporate the ReLU, our encoding step in (27) should be changed to

$$C = \rho(\Phi^\top \mathbb{H}_{d|p}(Z) \Psi).$$

Next, we consider a multi-layer convolutional framelets where the convolutional framelets are connected one-by-one. Here, at the first layer, (20) can be represented by

$$f = \mathbb{H}_{d_{(1)}}^\dagger (\tilde{\Phi}^{(1)} (\Phi^{(1)\top} \mathbb{H}_{d_{(1)}}(f) \Psi^{(1)}) \tilde{\Psi}^{(1)\top})$$

where the subscript and superscript index (l) represents the l -th layer. Similarly, we have

$$\Phi^{(1)\top} \mathbb{H}_{d_{(1)}}(f) \Psi^{(1)} = \mathbb{H}_{d_{(2)}|p_{(2)}}^\dagger (\tilde{\Phi}^{(2)} (\Phi^{(2)\top} \mathbb{H}_{d_{(2)}|p_{(2)}}(\Phi^{(1)\top} \mathbb{H}_{d_{(1)}}(f) \Psi^{(1)}) \Psi^{(2)}) \tilde{\Psi}^{(2)\top})$$

Thus, the two layer implementation is given by

$$f = \mathbb{H}_{d_{(1)}}^\dagger \left(\tilde{\Phi}^{(1)} \left(\mathbb{H}_{d_{(2)}|p_{(2)}}^\dagger (\tilde{\Phi}^{(2)} (\Phi^{(2)\top} \mathbb{H}_{d_{(2)}|p_{(2)}}(\Phi^{(1)\top} \mathbb{H}_{d_{(1)}}(f) \Psi^{(1)}) \Psi^{(2)}) \tilde{\Psi}^{(2)\top}) \right) \tilde{\Psi}^{(1)\top} \right)$$

In general, the L -layer implementation of the convolutional framelets with ReLU is given by

$$f = \mathbb{H}_{d_{(1)}}^\dagger \left(\tilde{\Phi}^{(1)} \dots \left(\mathbb{H}_{d_{(L)}|p_{(L)}}^\dagger (\tilde{\Phi}^{(L)} \rho(\Phi^{(L)\top} \mathbb{H}_{d_{(L)}|p_{(L)}} \dots \rho(\Phi^{(1)\top} \mathbb{H}_{d_{(1)}}(f) \Psi^{(1)}) \dots \Psi^{(L)}) \tilde{\Psi}^{(L)\top}) \right) \dots \tilde{\Psi}^{(1)\top} \right)$$

where $d_{(i)}$ and $p_{(i)}$ denotes the filter length and the number of input channels at the i -th layer, respectively.

Note that the number of input channels should increase exponentially across the layers to satisfy the PR

condition:

Proposition 4.7. *To achieve the PR condition, the number of Hankel blocks in the extended Hankel matrix in l -th layer, which corresponds to the number of signal to be filtered, should satisfy: $p_{(l)} = p_{(l-1)}d_{(l-1)} = \prod_{i=1}^l d_{(i-1)}$, with $p_{(0)} = 1 = d_{(0)}$ and $d_{(i)}$ is the filter length at the i -th layer. Accordingly, the minimum number of required filter channel at the l -th layer is given by*

$$p_{(l)}d_{(l)} = \prod_{i=0}^l d_{(i)}. \quad (28)$$

Proof. We prove this by mathematical induction. At $l = 1$, the input signal is $f \in \mathbb{R}^n$, so we need $\Phi^{(1)\top} \mathbb{H}_{d_{(1)}}(f) \Psi^{(1)}$ to obtain the filtered signal $C^{(1)}$. Since $\mathbb{H}_{d_{(1)}}(f) \in \mathbb{R}^{n \times d_{(1)}}$, $\Psi^{(1)} \in \mathbb{R}^{d_{(1)} \times d_{(1)}}$ and $p_{(1)} = 1$, this generates $p_{(2)} = d_{(1)}$ filtered output. At the l -th layer, we assume that (28) is true, which means that there are $p_{(l)}$ signals that needs to be filtered. Then, the filtering operation can be represented by (5) or $\Phi^{(l)\top} \mathbb{H}_{d_{(l)}|p_{(l)}}(f) \Psi^{(l)}$, where $\mathbb{H}_{d_{(l)}|p_{(l)}}(f) \in \mathbb{R}^{n \times p_{(l)}d_{(l)}}$. Thus, to guarantee the PR, the dimension of $\Psi^{(l)}$ should be $p_{(l)}d_{(l)} \times p_{(l)}d_{(l)}$. Therefore, the number of Hankel blocks in the $(l+1)$ -th layer should be $p_{(l+1)} = p_{(l)}d_{(l)}$. Q.E.D. \square

Due to the similarity of the multilayer implementation of the convolutional framelets to deep CNN networks, the training problem is similarly defined as follows.

Definition 4.1 (Deep Convolutional Framelets Training). *Let $\{f_i, y_i\}_{i=1}^N$ denote the input and target sample pairs. Then, the deep convolutional framelets training problem is given by*

$$\min_{\{\Phi^{(j)}, \tilde{\Phi}^{(j)}\}_{j=1}^L} \sum_{i=1}^N \|y_i - \mathbb{G}(f_i; \{\Phi^{(j)}, \tilde{\Phi}^{(j)}\}_{j=1}^L)\|^2 \quad (29)$$

where \mathbb{G} is defined by

$$\mathbb{G}(f_i; \{\Phi^{(j)}, \tilde{\Phi}^{(j)}\}_{j=1}^L) \quad (30)$$

$$= \mathbb{H}_{d_{(1)}}^\dagger \left(\tilde{\Phi}^{(1)} \dots \left(\mathbb{H}_{d_{(L)}|p_{(L)}}^\dagger \left(\tilde{\Phi}^{(L)} \rho \left(\Phi^{(L)\top} \mathbb{H}_{d_{(L)}|p_{(L)}} \dots \rho \left(\Phi^{(1)\top} \mathbb{H}_{d_{(1)}}(f) \Psi^{(1)} \dots \Psi^{(L)} \right) \tilde{\Psi}^{(L)\top} \right) \dots \tilde{\Psi}^{(1)\top} \right) \dots \right) \dots \right)$$

Note that if the target sample y_i is the same as the input f_i and the ReLU is not used, the training problem is nothing but the filter bank design problem to guarantee the PR. This is not usually the case in the standard deep learning because it does not usually satisfy the biorthogonal conditions (18) and (19). Therefore, in order to differentiate from the standard deep learning that always lose informations, we call the new network as *deep convolutional framelets*. Furthermore, even with the ReLU nonlinearity, we will later show that we can still guarantee the PR if sufficient number of filter channels are available.

B. Multi-resolution Analysis using Convolutional Framelets

In deep convolutional framelets, the non-local basis Φ , which is pre-determined by the applications, controls the overall structure. Among them, the perfect reconstruction multi-resolution analysis (MRA) using multi-layer implementation of convolutional framelets needs further discussion due to its importance. Here, we still use the standard pooling and unpooling networks, but there exists additional high-band paths that overcome the limitation of the existing pooling and unpooling.

One of the important motivations for multi-resolution analysis of convolutional framelets is due to the exponentially large receptive field. For example, Fig. 4 compares the network depth-wise effective receptive field for a multi-resolutinal network with pooling and a reference network without pooling layer. With the same size convolutional filters, the effective receptive field is enlarged in the network with pooling layers. Our MRA is derived to supplement the enlarged receptive field from pooling layers with the fine detailed processing using high-pass band convolutional framelets.

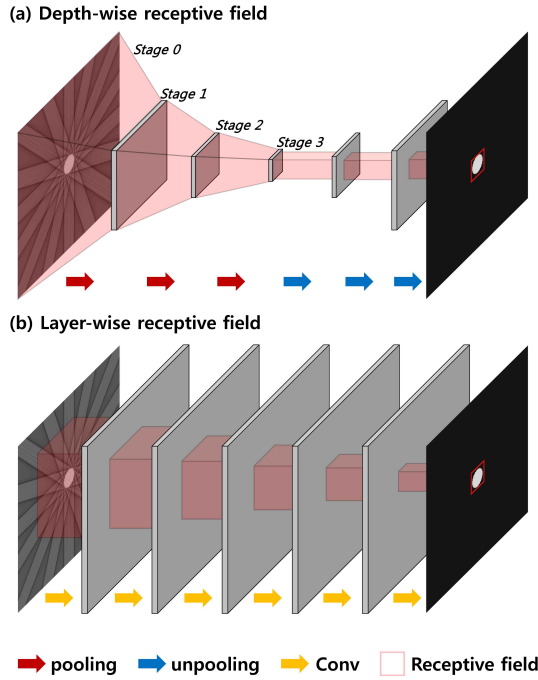


Fig. 4. Effective receptive field comparison.

Specifically, at the first layer, we are interested in learning the local basis $\Psi^{(1)}$ and its dual $\tilde{\Psi}^{(1)}$ such that

$$\mathbb{H}_{d_{(1)}}(f) = \Phi^{(1)} C^{(1)} \tilde{\Psi}^{(1)\top}, \quad \text{where} \quad C^{(1)} := \Phi^{(1)\top} \mathbb{H}_{d_{(1)}}(f) \Psi^{(1)}$$

For simplicity we assume that the nonlocal basis Φ is orthonormal. For MRA, we decompose the nonlocal

orthonormal basis $\Phi^{(1)}$ into the low and high frequency subbands, i.e.

$$\Phi^{(1)} = \begin{bmatrix} \Phi_{low}^{(1)} & \Phi_{high}^{(1)} \end{bmatrix} .$$

For example, if we use Haar wavelet, the first layer operator $\Phi_{low}^{(1)}, \Phi_{high}^{(1)} \in \mathbb{R}^{n \times \frac{n}{2}}$ are given by

$$\Phi_{low}^{(1)} = \frac{1}{\sqrt{2}} \begin{bmatrix} 1 & 0 & \cdots & 0 \\ 1 & 0 & \cdots & 0 \\ 0 & 1 & \cdots & 0 \\ 0 & 1 & \cdots & 0 \\ \vdots & \vdots & \ddots & \vdots \\ 0 & 0 & \cdots & 1 \\ 0 & 0 & \vdots & 1 \end{bmatrix}, \quad \Phi_{high}^{(1)} = \frac{1}{\sqrt{2}} \begin{bmatrix} 1 & 0 & \cdots & 0 \\ -1 & 0 & \cdots & 0 \\ 0 & 1 & \cdots & 0 \\ 0 & -1 & \cdots & 0 \\ \vdots & \vdots & \ddots & \vdots \\ 0 & 0 & \cdots & 1 \\ 0 & 0 & \vdots & -1 \end{bmatrix}$$

Note that $\Phi_{low}^{(1)}$ is exactly the same as the average pooling operation in (23), but $\Phi^{(1)} = \begin{bmatrix} \Phi_{low}^{(1)} & \Phi_{high}^{(1)} \end{bmatrix}$ now constitutes an orthonormal basis in \mathbb{R}^n .

We also define the approximate signal $C_{low}^{(1)}$ and the detail signal $C_{high}^{(1)}$:

$$C_{low}^{(1)} := \Phi_{low}^{(1)\top} \mathbb{H}_{d_{(1)}}(f) \Psi^{(1)}, \quad C_{high}^{(1)} := \Phi_{high}^{(1)\top} \mathbb{H}_{d_{(1)}}(f) \Psi^{(1)}$$

such that

$$C^{(1)} = \Phi^{(1)\top} \mathbb{H}_{d_{(1)}}(f) \Psi^{(1)} = \begin{bmatrix} C_{low}^{(1)} \\ C_{high}^{(1)} \end{bmatrix}$$

Note that this operation corresponds to the local filtering followed by non-local transform as shown in the red block of Fig. 5. Then, at the first layer, we have the following decomposition:

$$\mathbb{H}_{d_{(1)}}(f) = \Phi^{(1)} C^{(1)} \tilde{\Psi}^{(1)\top} = \Phi_{low}^{(1)} C_{low}^{(1)} \tilde{\Psi}^{(1)\top} + \Phi_{high}^{(1)} C_{high}^{(1)} \tilde{\Psi}^{(1)\top}$$

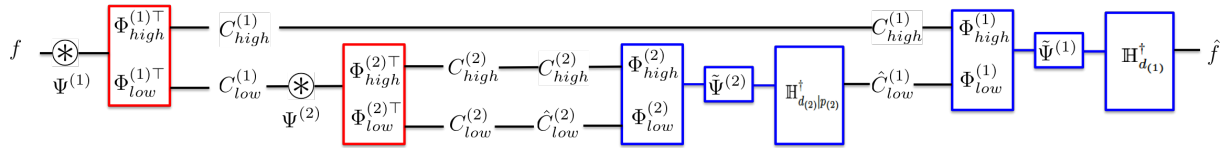


Fig. 5. Proposed multi-resolution analysis of deep convolutional framelets. Here, \otimes corresponds to the convolution operation; the red and blue blocks corresponds to the encoder and decoder blocks, respectively.

At the second layer, we proceed similarly using the approximate signal $C_{low}^{(1)}$. More specifically, we are interested in using orthonormal non-local transform: $\Phi^{(2)} = [\Phi_{low}^{(2)} \quad \Phi_{high}^{(2)}]$, where $\Phi_{low}^{(2)}$ and $\Phi_{high}^{(2)}$ transforms the approximate signal $C_{low}^{(1)} \in \mathbb{R}^{n/2 \times d_{(1)}}$ to low and high bands, respectively (see Fig. 5):

$$\mathbb{H}_{d_{(2)}|p_{(2)}}(C_{low}^{(1)}) = \Phi_{low}^{(2)} C_{low}^{(2)} \tilde{\Psi}^{(2)\top} + \Phi_{high}^{(2)} C_{high}^{(2)} \tilde{\Psi}^{(2)\top},$$

where $p_{(2)} = d_{(1)}$ denotes the number of Hankel blocks in (6), $d_{(2)}$ is the second layer convolution filter

length, and

$$C_{low}^{(2)} := \Phi_{low}^{(2)\top} \mathbb{H}_{d_{(2)}|p_{(2)}}(C_{low}^{(1)}) \Psi^{(2)} \quad , \quad C_{high}^{(2)} := \Phi_{high}^{(2)\top} \mathbb{H}_{d_{(2)}|p_{(2)}}(C_{low}^{(1)}) \Psi^{(2)} \quad (31)$$

Again, $\Phi_{low}^{(2)}$ corresponds to the standard average pooling operation. Note that we need a lifting operation to an extended Hankel matrix with $p_{(2)} = d_{(1)}$ Hankel blocks in (31), because the first layers generates $p_{(2)}$ filtered output which needs to be convolved with $d_{(2)}$ -length filters in the second layer.

Similarly, the approximate signal needs further processing from the following layers. In general, for $l = 1, \dots, L$, we have

$$\mathbb{H}_{d_{(l)}|p_{(l)}}(C_{low}^{(l-1)}) = \Phi_{low}^{(l)} C_{low}^{(l)} \tilde{\Psi}^{(l)\top} + \Phi_{high}^{(l)} C_{high}^{(l)} \tilde{\Psi}^{(l)\top},$$

where

$$C_{low}^{(l)} := \Phi_{low}^{(l)\top} \mathbb{H}_{d_{(l)}|p_{(l)}}(C_{low}^{(l-1)}) \Psi^{(l)} \quad , \quad C_{high}^{(l)} := \Phi_{high}^{(l)\top} \mathbb{H}_{d_{(l)}|p_{(l)}}(C_{low}^{(l-1)}) \Psi^{(l)}$$

where $p_{(l)} = p_{(l-1)}d_{(l-1)}$ denotes the dimension of local basis at l -th layer. This results in L -layer deep convolutional framelets using Haar wavelet.

The multilayer implementation of convolutional framelets now results in an interesting encoder-decoder deep network structure as shown in Fig. 5, where the red and blue blocks represent encoder and decoder blocks, respectively. In addition, Table I summarizes the dimension of the l -th layer matrices. More specifically, with the ReLU, the encoder parts are given as follows:

$$\left\{ \begin{array}{ll} C_{low}^{(1)} = \rho \left(\Phi_{low}^{(1)\top} \mathbb{H}_{d_{(1)}}(f) \Psi^{(1)} \right), & C_{high}^{(1)} = \Phi_{high}^{(1)\top} \mathbb{H}^{d_{(1)}} \Psi^{(1)} \\ C_{low}^{(2)} = \rho \left(\Phi_{low}^{(2)\top} \mathbb{H}_{d_{(2)}|p_{(2)}}(C_{low}^{(1)}) \Psi^{(2)} \right), & C_{high}^{(2)} = \Phi_{high}^{(2)\top} \mathbb{H}_{d_{(2)}|p_{(2)}}(C_{low}^{(1)}) \Psi^{(2)} \\ & \vdots \\ C_{low}^{(L)} = \rho \left(\Phi_{low}^{(L)\top} \mathbb{H}_{d_{(L)}|p_{(L)}}(C_{low}^{(L-1)}) \Psi^{(L)} \right), & C_{high}^{(L)} = \Phi_{high}^{(L)\top} \mathbb{H}_{d_{(L)}|p_{(L)}}(C_{low}^{(L-1)}) \Psi^{(L)} \end{array} \right.$$

which corresponds to multi-channel filtering with local filter $\Psi^{(l)} \in \mathbb{R}^{p_{(l)}d_{(l)} \times p_{(l)}d_{(l)}}$ followed by the non-local transform $\Phi_{high}^{(l)\top}$ or $\Phi_{low}^{(l)\top}$. On the other hand, the decoder part is given by

$$\left\{ \begin{array}{ll} \hat{C}_{low}^{(L-1)} = \rho \left(\mathbb{H}_{d_{(L)}|p_{(L)}}^\dagger \left(\Phi^{(L)} \hat{C}^{(L)} \tilde{\Psi}^{(L)\top} \right) \right) \\ \hat{C}_{low}^{(L-2)} = \rho \left(\mathbb{H}_{d_{(L-1)}|p_{(L-1)}}^\dagger \left(\Phi^{(L-1)} \hat{C}^{(L-1)} \tilde{\Psi}^{(L-1)\top} \right) \right) \\ \vdots \\ \hat{C}_{low}^{(1)} = \rho \left(\mathbb{H}_{d_{(2)}|p_{(2)}}^\dagger \left(\Phi^{(2)} \hat{C}^{(2)} \tilde{\Psi}^{(2)\top} \right) \right) \\ \hat{f} = \mathbb{H}_{d_{(1)}}^\dagger \left(\Phi^{(1)} \hat{C}^{(1)} \tilde{\Psi}^{(1)\top} \right) \end{array} \right. \quad (32)$$

where we use

$$\Phi^{(l)} \hat{C}^{(l)} \tilde{\Psi}^{(l)\top} = \Phi_{low}^{(l)} \hat{C}_{low}^{(l)} \tilde{\Psi}^{(l)\top} + \Phi_{high}^{(l)} C_{high}^{(l)} \tilde{\Psi}^{(l)\top}.$$

Here, $C_{high}^{(l)}$ is a direct output from the encoder at the same layer, whereas $\hat{C}_{low}^{(l)}$ is the decoded low frequency

band from $(l + 1)$ -th resolution layer (except that $\hat{C}_{low}^{(L)} = C_{low}^{(L)}$). Note that ReLU is only used for the low-frequency branch to enforce the consistency between the encoder and decoder.

Name	Symbol	Dimension
Non-local basis	$\Phi^{(l)}$	$\frac{n}{2^{l-1}} \times \frac{n}{2^{l-1}}$
Low-band non-local basis	$\Phi_{low}^{(l)}$	$\frac{n}{2^{l-1}} \times \frac{n}{2^l}$
High-band non-local basis	$\Phi_{high}^{(l)}$	$\frac{n}{2^{l-1}} \times \frac{n}{2^l}$
Local basis	$\Psi^{(l)}$	$p_{(l)}d_{(l)} \times p_{(l)}d_{(l)}$
Dual local basis	$\tilde{\Psi}^{(l)}$	$p_{(l)}d_{(l)} \times p_{(l)}d_{(l)}$
Signal and its estimate	$C^{(l)}, \hat{C}^{(l)}$	$\frac{n}{2^{l-1}} \times p_{(l)}d_{(l)}$
Approximate signal and its estimate	$C_{low}^{(l)}, \hat{C}_{low}^{(l)}$	$\frac{n}{2^l} \times p_{(l)}d_{(l)}$
Detail signal	$C_{high}^{(l)}$	$\frac{n}{2^l} \times p_{(l)}d_{(l)}$
Hankel lifting of low-band signals	$\mathbb{H}_{d_{(l)} p_{(l)}}(C_{low}^{(l-1)})$	$\frac{n}{2^{l-1}} \times p_{(l)}d_{(l)}$

TABLE I

THE NOMENCLATURE AND DIMENSIONS OF THE MATRICES AT THE l -TH LAYER MRA USING DEEP CONVOLUTIONAL FRAMELET. HERE, $d_{(l)}$ DENOTES THE FILTER LENGTH, AND $p_{(l)} = p_{(l-1)}d_{(l-1)}$ WITH $p_{(0)} = d_{(0)} = 1$ REFERS TO THE NUMBER OF HANKEL BLOCK.

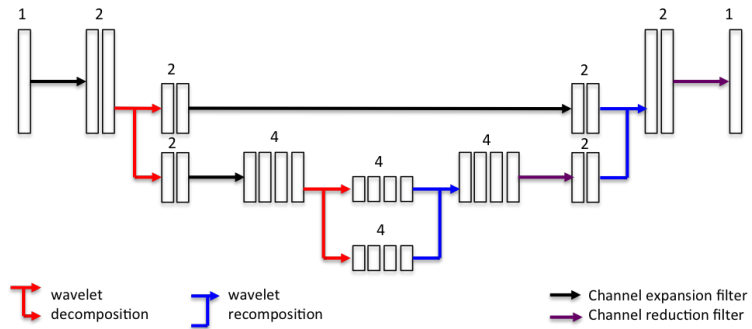


Fig. 6. A multi-resolution deep convolutional framelet decomposition with a length-2 local filters.

Fig. 6 shows the overall convolutional framelet structure when length-2 local filters are used. Note that the structure is quite similar to U-net structure, except the high pass filter pass. This again confirms a close relationship between the deep convolutional framelets and deep neural networks.

C. Role of Nonlinearity

Recall that the PR condition for the deep convolutional framelets was derived without assuming any nonlinearity. Thus, the introduction of ReLU appears counter-intuitive in the context of PR. Amazingly, in spite of ReLU nonlinearity, the following theorem shows that the PR condition can be satisfied when redundant filter channels are available. Here, by redundant filter channels, we refer the case with $\Psi \in \mathbb{R}^{d \times 2m}$ where $m \geq d$ as shown in Fig. 7.

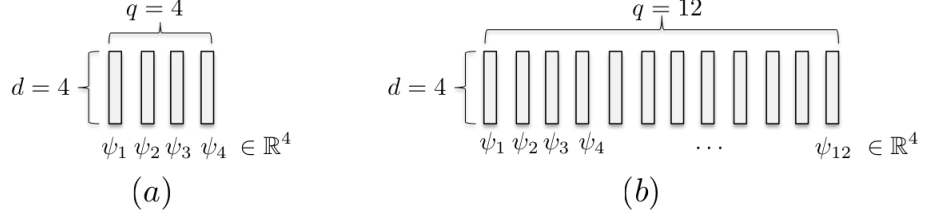


Fig. 7. (a) Complete set of local filters, and (b) redundant local filters.

Theorem 4.8 (PR under ReLU using Redundant Filter Channels). *Consider the training problem in (29) with $y_i = f_i$ for all $i = 1, \dots, N$. Suppose, furthermore, $\tilde{\Phi}^{(l)\top} \Phi^{(l)\top} = I_{n \times n}$ and $\Psi^{(l)}, \tilde{\Psi}^{(l)} \in \mathbb{R}^{p_{(l)} d_{(l)} \times 2m_{(l)}}$ with $m_{(l)} \geq p_{(l)} d_{(l)}$ for all $l = 1, \dots, L$. Then, one of the solutions for the optimization problem (29) is given by*

$$\Psi^{(l)} = \begin{bmatrix} \Psi_1^{(l)} & -\Psi_1^{(l)} \end{bmatrix}, \quad \tilde{\Psi}^{(l)} = \begin{bmatrix} \tilde{\Psi}_1^{(l)} & -\tilde{\Psi}_1^{(l)} \end{bmatrix} \quad \forall l = 1, \dots, L, \quad (33)$$

with

$$\Psi_i^{(l)\top} \tilde{\Psi}_i^{(l)\top} = I_{d \times d}, \quad \Psi_i^{(l)}, \tilde{\Psi}_i^{(l)} \in \mathbb{R}^{p_{(l)} d_{(l)} \times m_{(l)}}$$

which guarantees the PR, i.e.

$$f_i = \mathbb{G} \left(f_i; \{\Phi^{(j)}, \tilde{\Phi}^{(j)}\}_{j=1}^L \right), \quad \forall i.$$

Proof. We will prove by construction. Let $F^{(l)} := \Pi_{d_{(l)}|p_{(l)}}(C^{(l)})$. Because $\Phi^{(l)\top} F^{(l)}(-\Psi_1^{(l)}) = -\Phi^{(l)\top} F^{(l)} \Psi_1^{(l)}$, the negative part can be retrieved from $-\rho(\Phi^{(l)\top} F^{(l)}(-\Psi_1^{(l)}))$, while only positive part of $\Phi^{(l)\top} F^{(l)} \Psi_1^{(l)}$ can be retained from $\rho(\Phi^{(l)\top} F^{(l)} \Psi_1^{(l)})$. Furthermore, their non-zero parts do not overlap.

Thus,

$$\Phi^{(l)\top} F^{(l)} \Psi_1^{(l)} = \rho(\Phi^{(l)\top} F^{(l)} \Psi_1^{(l)}) - \rho(\Phi^{(l)\top} F^{(l)}(-\Psi_1^{(l)})). \quad (34)$$

Accordingly, by choosing (33), we have

$$\begin{aligned} \Phi^{(l)} \rho(\Phi^{(l)\top} F^{(l)} \Psi^{(l)}) \Psi^{(l)\top} &= \Phi^{(l)} \left[\rho(\Phi^{(l)\top} F^{(l)} \Psi_1^{(l)}) - \rho(\Phi^{(l)\top} F^{(l)}(-\Psi_1^{(l)})) \right] \begin{bmatrix} \tilde{\Psi}_i^{(l)\top} \\ -\tilde{\Psi}_i^{(l)\top} \end{bmatrix} \\ &= \Phi^{(l)} \left(\rho(\Phi^{(l)\top} F^{(l)} \Psi_1^{(l)}) - \rho(\Phi^{(l)\top} F^{(l)}(-\Psi_1^{(l)})) \right) \tilde{\Psi}_i^{(l)\top} \\ &= \Phi^{(l)} \Phi^{(l)\top} F^{(l)} \Psi_1^{(l)} \tilde{\Psi}_i^{(l)\top} \\ &= F^{(l)} \end{aligned}$$

where we use (34) for the third inequality. By applying this from $l = 1$ to L to (30), we can see that $f_i = \mathbb{G} \left(f_i; \{\Phi^{(j)}, \tilde{\Phi}^{(j)}\}_{j=1}^L \right)$. Q.E.D. \square

Remark 4.9. *Eq. (33) in Theorem 4.8 predicts the existence of filter pairs with opposite phase. Amazingly, this theoretical prediction coincides with the empirical observation in deep learning literature. For example,*

Shang *et al* [50] observed an intriguing property that the filters in the lower layers form pairs (i.e., filters with opposite phase). To exploit this property for further network performance improvement, the authors proposed so called concatenated ReLU (CRelu) to explicitly retrieve the negative part of $\Phi^\top F \Psi_1$ using $\rho(\Phi^\top F(-\Psi_1))$ [50].

Remark 4.10. Note that (33) informs that there are infinite number of global minimizers for the minimization problem (29). In fact, the most important requirement for PR is the existence of opposite phase filters as in (33) rather than the specific filter coefficients. This may suggest the excellent generalization performance of a deep network even from small set of training data set.

Theorem 4.8 deals with the PR condition with the redundant local filters $\Psi \in \mathbb{R}^{pd \times 2m}$ with $m \geq pd$. This can be easily satisfied at the lower layers of the deep convolutional framelets; however, the number of filter channels for PR grows exponentially according to layers as shown in (28). Thus, at higher layers of deep convolutional framelets, the condition for Theorem 4.8 cannot be satisfied. The following theorem shows the effect of such insufficient filter channels:

Theorem 4.11 (Low-Rank Approximation with Insufficient Filter Channels). For a given input $C \in \mathbb{R}^{n \times p}$, let $\mathbb{H}_{d|p}(C)$ denotes its extended Hankel matrix and its SVD is given by

$$\mathbb{H}_{d|p}(C) = U \Sigma V^\top = \sum_{i=1}^{pd} \sigma_i u_i v_i^\top, \quad (35)$$

where u_i and v_i denotes the left and right singular vectors, and $\sigma_1 \geq \sigma_2 \geq \dots \geq \sigma_{pd} \geq 0$ are the singular values. Suppose, furthermore, that $\tilde{\Phi} \Phi^\top = I_{n \times n}$. Then, for a given basis $\Psi = [\Psi_1, \Psi_2] \in \mathbb{R}^{pd \times 2m}$ and dual basis $\tilde{\Psi} = [\tilde{\Psi}_1, \tilde{\Psi}_2] \in \mathbb{R}^{pd \times 2m}$ with $m < pd$ such that it satisfies (33), the solution for the following optimization problem:

$$\min_{\Psi, \tilde{\Psi}} \|\mathbb{H}_{d|p}(C) - \Phi \rho(\Phi^\top \mathbb{H}_{d|p}(C) \Psi) \tilde{\Psi}^\top\|_F^2 \quad (36)$$

is given by

$$\Psi_1 = \tilde{\Psi}_1 = V_{1:m} = [v_1 \ \dots \ v_m],$$

and

$$\Phi \rho(\Phi^\top \mathbb{H}_{d|p}(C) \Psi) \tilde{\Psi}^\top = \mathbb{H}_{d|p}(C) P_{R(V_{1:m})},$$

which is the rank m -projection.

Proof. From the proof of Theorem 4.8, we know that

$$\Phi \rho(\Phi^\top \mathbb{H}_{d|p}(C) [\Psi_1 \ - \Psi_1]) \begin{bmatrix} \tilde{\Psi}_1^\top \\ -\tilde{\Psi}_1^\top \end{bmatrix} = \Phi \Phi^\top \mathbb{H}_{d|p}(C) \Psi_1 \tilde{\Psi}_1^\top = \mathbb{H}_{d|p}(C) \Psi_1 \tilde{\Psi}_1^\top,$$

where the last equality comes from the orthonormality of Φ . Thus, (36) can be simplified as

$$\begin{aligned} \min_{\Psi_1, \tilde{\Psi}_1} \|\mathbb{H}_{d|p}(C) - \mathbb{H}_{d|p}(C)\Psi_1 \tilde{\Psi}_1^\top\|_F^2 &= \min_{\Psi_1, \tilde{\Psi}_1} \|\mathbb{H}_{d|p}(C)(I_{pd \times pd} - \Psi_1 \tilde{\Psi}_1^\top)\|_F^2 \\ &= \min_{\Psi_1, \tilde{\Psi}_1} \|U\Sigma V^\top(I_{pd \times pd} - \Psi_1 \tilde{\Psi}_1^\top)\|_F^2 \\ &= \min_{\Psi_1, \tilde{\Psi}_1} \|\Sigma V^\top(I_{pd \times pd} - \Psi_1 \tilde{\Psi}_1^\top)\|_F^2 \end{aligned}$$

Thus, to have the minimum cost value, $\Psi_1 \tilde{\Psi}_1^\top = V_{1:m} V_{1:m}^\top$, where $V_{1:m} = [v_1 \ \dots \ v_m]$. Thus, by choosing $\Psi_1 = \tilde{\Psi}_1 = V_{1:m}$, we conclude the proof. \square

We believe that Theorem 4.11 is very important, because it shows the origin of the power of deep learning in the context of inverse problem. More specifically, the lower layers perform signal decomposition using various filter bank satisfying the PR conditions, after which high layers of deep network exploit the joint sparsity between the channels using low-rank approximation of extended Hankel matrix. We conjecture that the deep network is trained such that the signal decomposition as well as low-rank approximation is optimally fitted to the desired input/output relationship.

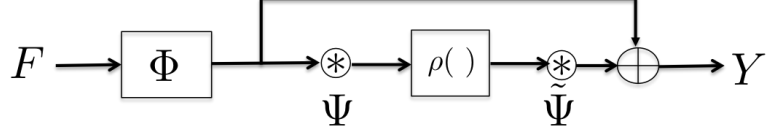


Fig. 8. Block diagram of a residual block.

The low-rank approximation is good for reducing the noises. Thus, the small number of channels are usually inserted in convolutional framelets as shown in Fig. 3(a)(b). However, as the network gets deeper, more layers cannot satisfy the condition (28). Thus, successive applications of the CNN can reduce the important signals. To address this, the residual net [47] is useful. Recall that the residual net (ResNet) has been widely used for image classification as well as image reconstruction. More specifically, the residual net architecture shown in Fig. 8 can be represented by

$$Y = R(F; \Phi, \Psi, \tilde{\Psi}) := \Phi^\top F - \rho(\Phi^\top F \Psi) \tilde{\Psi}^\top \quad (37)$$

where $F := \mathbb{H}_{d|p}(C)$. The following result shows that the residual network works as high rank approximation to truncate the least significant subspaces:

Theorem 4.12 (High-Rank Approximation using Residual Nets). *For a given input $C \in \mathbb{R}^{n \times p}$, let $\mathbb{H}_p^d(C)$ denotes its extended Hankel matrix and its SVD is given by (35). Suppose, furthermore, that $\tilde{\Phi}\Phi^\top = I_{n \times n}$. Then, for a given basis $\Psi = [\Psi_1, \Psi_2] \in \mathbb{R}^{pd \times 2m}$ and dual basis $\tilde{\Psi} = [\tilde{\Psi}_1, \tilde{\Psi}_2] \in \mathbb{R}^{pd \times 2m}$ with $m < pd$ such*

that it satisfies (33), the solution for the residual network optimization problem:

$$\min_{\Psi, \tilde{\Psi}} \|\Phi^\top \mathbb{H}_{d|p}(C) - R(F; \Phi, \Psi, \tilde{\Psi})\|_F^2 \quad (38)$$

is given by

$$\Psi_1 = \tilde{\Psi}_1 = V_{pd-m+1:pd} := [v_{pd-m+1} \ \cdots \ v_{pd}],$$

and

$$R(F; \Phi, \Psi, \tilde{\Psi}) = \Phi^\top \mathbb{H}_{d|p}(C) P_{R(V_{pd-m+1:pd})}^\perp = \Phi^\top \mathbb{H}_{d|p}(C) P_{R(V_{1:pd-m})},$$

which is the rank $(pd - m)$ projection.

Proof. From the proof of Theorem 4.8, we know that

$$\rho(\Phi^\top \mathbb{H}_{d|p}(C)[\Psi_1 - \tilde{\Psi}_1]) \begin{bmatrix} \tilde{\Psi}_1^\top \\ -\tilde{\Psi}_1^\top \end{bmatrix} = \Phi^\top \mathbb{H}_{d|p}(C) \Psi_1 \tilde{\Psi}_1^\top = \Phi^\top \mathbb{H}_{d|p}(C) \Psi_1 \tilde{\Psi}_1^\top.$$

Thus, (38) can be simplified as

$$\begin{aligned} \min_{\Psi_1, \tilde{\Psi}_1} \|\Phi^\top \mathbb{H}_{d|p}(C) - R(F; \Phi, \Psi_1, \tilde{\Psi}_1)\|_F^2 &= \min_{\Psi_1, \tilde{\Psi}_1} \|\Phi^\top \mathbb{H}_{d|p}(C) - \Phi^\top \mathbb{H}_{d|p}(C) + \Phi^\top \mathbb{H}_{d|p}(C)(\Psi_1 \tilde{\Psi}_1^\top)\|_F^2 \\ &= \min_{\Psi_1, \tilde{\Psi}_1} \|\Phi^\top \mathbb{H}_{d|p}(C)(\Psi_1 \tilde{\Psi}_1^\top)\|_F^2 \\ &= \min_{\Psi_1, \tilde{\Psi}_1} \|\mathbb{H}_{d|p}(C)(\Psi_1 \tilde{\Psi}_1^\top)\|_F^2 \\ &= \min_{\Psi_1, \tilde{\Psi}_1} \|U \Sigma V^\top \Psi_1 \tilde{\Psi}_1^\top\|_F^2 \end{aligned}$$

Thus, to have the minimum cost value, $\Psi_1 \tilde{\Psi}_1^\top = V_{pd-m+1:pd} V_{pd-m+1:pd}^\top$, where $V_{pd-m+1:pd} = [v_{pd-m+1} \ \cdots \ v_{pd}]$. Thus, we choose $\Psi_1 = \tilde{\Psi}_1 = V_{pd-m+1:pd}$. Finally, this results in the following:

$$\begin{aligned} R(F; \Phi, \Psi, \tilde{\Psi}) &= \Phi^\top \mathbb{H}_{d|p}(C) - \Phi^\top \mathbb{H}_{d|p}(C) P_{R(V_{pd-m+1:pd})}^\perp \\ &= \Phi^\top \mathbb{H}_{d|p}(C) P_{R(V_{pd-m+1:pd})}^\perp \\ &= \Phi^\top \mathbb{H}_{d|p}(C) P_{R(V_{1:pd-m})} \end{aligned}$$

Q.E.D. □

D. Case Study: Existing Deep Network for Inverse Problems

In the following, we discuss some special cases of deep convolutional framelets, which correspond to the specific examples of existing deep learning architectures for inverse problems.

1) *Wavelet Residual Network (WavResNet)*: Kang et al [11] proposed a wavelet domain residual learning (WavResNet) for low-dose CT reconstruction combined with multiple residual blocks as shown in Fig. 9. The key idea of WavResNet is to apply the directional wavelet transform first, after which a neural network is trained such that it can learn the mapping between noisy input wavelet coefficients and noiseless ones

[11]. In essence, this can be interpreted as a deep convolutional framelets after the nonlocal transform is performed first using directional wavelets, and the remaining layers are composed of CNN with local filters and residual blocks. Thanks to the global transform using directional wavelets, the signal becomes sparse, which is the main source of the advantages compared to the simple CNN. However, due to the lack of pooling layers, the receptive field size is smaller than that of U-net. Accordingly, the architecture was better suited for localized artifacts from low-dose CT noise, but it is not effective for removing globalized artifact patterns from sparse view CT.

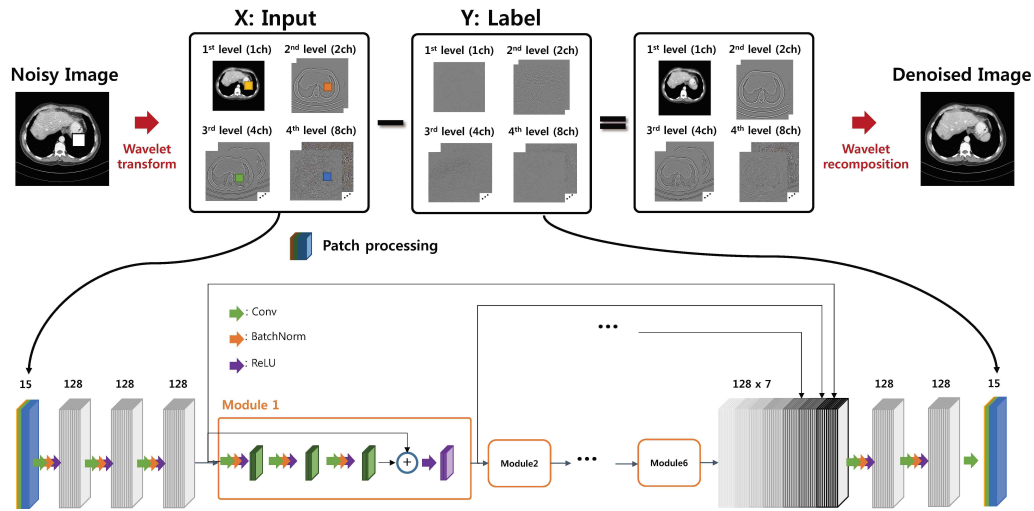


Fig. 9. WavResNet architecture for low-dose CT reconstruction [11].

2) *AUTOMAP*: AUtomated TransfOrm by Manifold APproximation (AUTOMAP) [51] is a recently proposed neural network approach for image reconstruction, which is claimed to be general for various imaging modalities such as MRI, CT, etc. A typical architecture is given in Fig. 10. This architecture is similar to Fig. 9, except that the first layer nonlocal transform $\Phi^{(1)}$ is learned as a fully connected layer. Moreover, the original signal domain is the measurement domain, so only local filters are followed in successive layer without additional fully connected layer for inversion. In theory, if $\Phi^{(1)}$ is learned to make $\Phi^{(1)\top} \mathbb{H}_d(f)$ to be sufficiently sparse, then it is believed to be the advantageous over standard CNN.

However, in order to use the fully connected layer as the nonlocal transform, a huge size network is required. For example, as shown in Fig. 10, in order to recover $N \times N$ image, the number of parameters for the fully connected layer is $2N^2 \times N^2$ (see [51] for more calculation of required parameter numbers). Thus, if one attempts to learn the CT image of size 512×512 (i.e. $N = 2^9$) using AUTOMAP, the required memory becomes $2N^4 = 2^{37}$, which is neither possible to store nor to avoid any overfitting during the learning.

This is another reason we propose to use analytic nonlocal transform such as wavelets, because wavelet

transforms do not need to be stored or learned but still provides near optimal nonlocal transform for piecewise smooth functions [20].

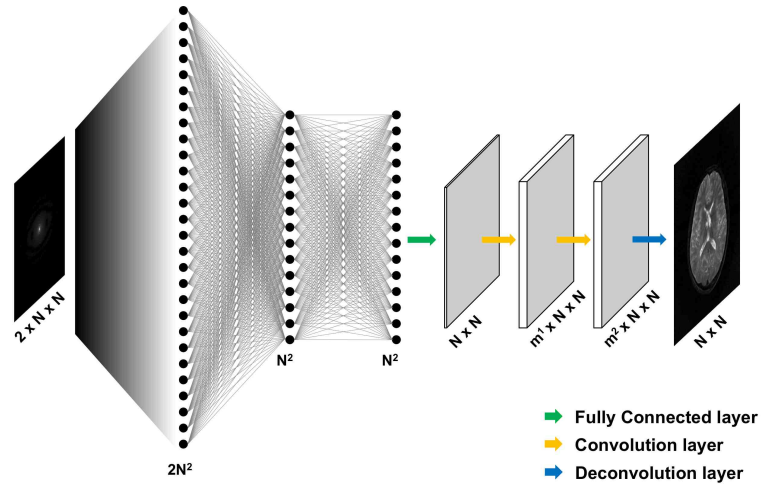


Fig. 10. AUTOMAP architecture [51].

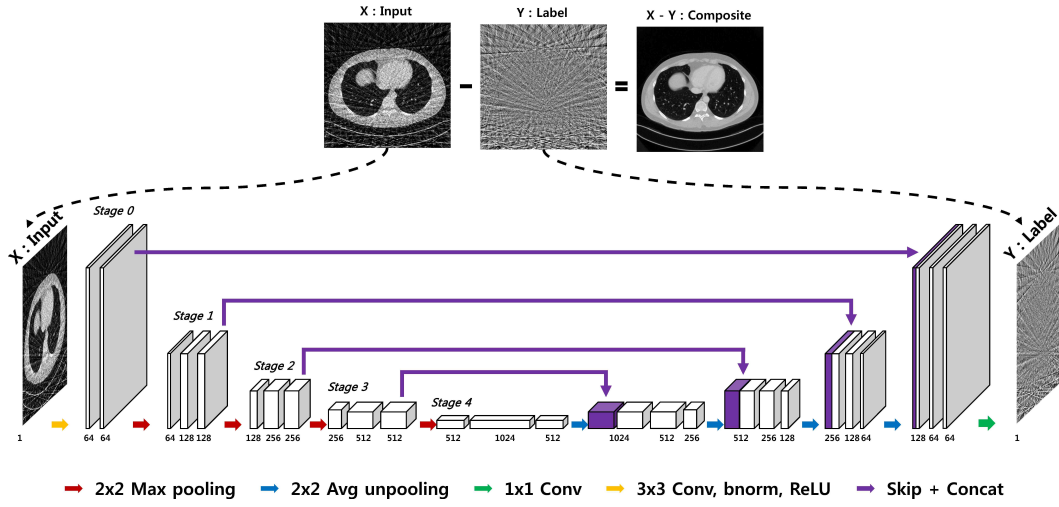


Fig. 11. U-net architecture for sparse view CT reconstruction [15].

3) *U-Net architecture*: The U-net is composed of encoder and decoder network with skipped connection. The encoder and decoder network utilizes the pooling and unpooling as shown in Fig. 11. As discussed before, the pooling and unpooling layers corresponds to the low-pass filtering of the input signals and the application of the short length filters further approximates the signal using low-rank or sparse approximation. On the other hand, the skipped connection works as residual network, so the net effect is to truncate the least significant transform coefficients and low-frequency signals. Therefore, this network works very well with

estimating globalized artifacts such as streaking artifacts, etc [14], [15]. However, the detailed information is often lost during pooling, so it is not as effective as WavResNet in removing localized noises.

E. Multi-Resolution Deep Convolutional Framelets for Inverse Problems

Based on the discussion so far, we propose a new class of deep learning network using multi-resolution deep convolutional framelets, which is believed to be quite universal for various inverse problems. For the applications of image reconstruction, our deep convolutional framelets is extended to 2-D structure, and the proposed architecture is illustrated in Fig. 12. The proposed network is basically obtained from multi-resolutional convolutional framelet architecture using 2-D Haar wavelet. Furthermore, the redundant filter channels are added between each layers, enabling accurate recovery of high-band and low-band signals at the same time.

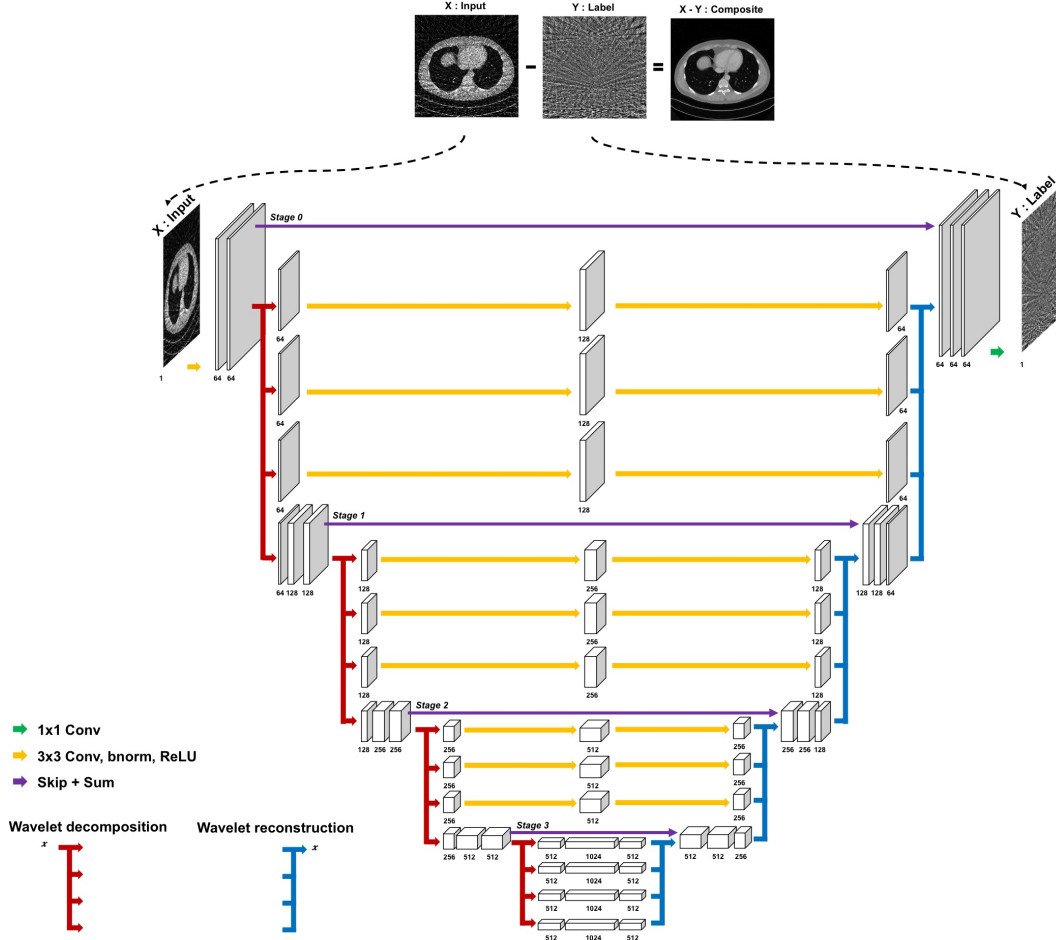


Fig. 12. Proposed multi-resolution deep convolutional framelet decomposition.

V. EXPERIMENTAL RESULTS

A. Methods

In order to evaluate the performance of the proposed deep convolutional framelets for inverse problems, a challenging problems of sparse view x-ray computed tomography (CT) problem is used. More specifically, in X-ray CT, due to the potential risk of radiation exposure, the main research thrust is to reduce the radiation dose. Among various approaches for low-dose CT, sparse-view CT is a recent proposal that reduces the radiation dose by reducing the number of projection views [52]. However, due to the insufficient projection views, standard reconstruction using the filtered back-projection (FBP) algorithm exhibits severe streaking artifacts that are globally distributed. Accordingly, researchers have extensively employed compressed sensing approaches [53] that minimize the the total variation (TV) or other sparsity-inducing penalties under the data fidelity [52]. These approaches are, however, computationally very expensive due to the repeated applications of projection and back-projection during iterative update steps.

Therefore, the main goal of this experiment is to apply the proposed network for sparse view CT reconstruction that outperforms the existing approaches in its computational speed as well as reconstruction quality. To address this, our network is trained to learn streaking artifacts as suggested in [15], which is in fact equivalent to learn images with a skipped connection [14]. Once the streaking artifacts are estimated, an artifact-free image is then obtained by subtracting the estimated streaking artifacts as shown in Fig. 12.

As a training data, we used the ten patient data provided by AAPM Low Dose CT Grand Challenge (<http://www.aapm.org/GrandChallenge/LowDoseCT/>). The data is composed of 3-D CT projection data from 2304 views. Artifact-free original images were generated by FBP using all 2304 projection views. Sparse view reconstruction input images X were generated using FBP from 48, 64, 96, and 192 projection views, respectively. For the proposed residual learning, the label data Y were defined as the difference between the sparse view reconstruction and the full view reconstruction.

Among the ten patient data, eight patient data were used for training, one patient data was used for validation, whereas a test was conducted using the remaining another patient data. This corresponding to 3602 and 504 slices of 512×512 images for the training and validation data, respectively, and 488 slices of 512×512 images for the test data. The training data was augmented by conducting horizontal and vertical flipping. For the training data set, we used the FBP reconstruction using 48, 96, and 196 projection views simultaneously as input X and the difference between the full view (2304 views) reconstruction and the sparse view reconstructions were used as label Y .

As for the baseline network for comparison, we use the U-net structure in Fig. 11 [15] and a single resolution CNN. The single resolution CNN has the same architecture with U-net in Fig. 11, except that

pooling and unpooling were not used. All these network were trained similarly using the same data set. For quantitative evaluation, we use the normalized mean square error (NMSE), which is defined as

$$NMSE = \frac{\sum_{i=1}^N \sum_{j=1}^N [x(i, j) - \hat{x}(i, j)]^2}{\sum_{i=1}^N \sum_{j=1}^N [x(i, j)]^2}, \quad (39)$$

where \hat{x} is the reconstructed X-ray CT images from sparse view and x is a full-view reconstruction image (ground truth).

The proposed network was trained by stochastic gradient descent (SGD). The regularization parameter was $\lambda = 10^{-4}$. The learning rate was set from 10^{-3} to 10^{-5} which was gradually reduced at each epoch. The number of epoch was 100. A mini-batch data using image patch was used, and the size of image patch was 256×256 . The network was implemented using MatConvNet toolbox (ver.24) [54] in MATLAB 2015a environment (Mathwork, Natick). We used a GTX 1080 graphic processor and i7-4770 CPU (3.40GHz). The network takes about 4 days for training.

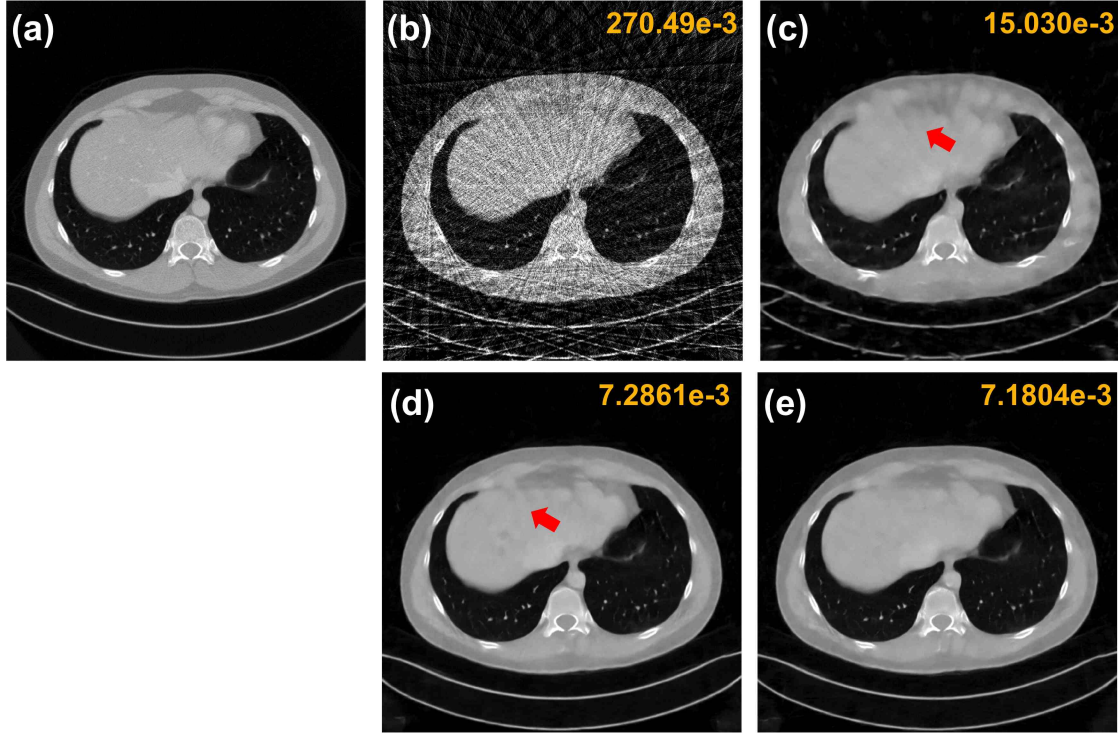


Fig. 13. CT reconstruction results for single scale CNN, U-Net and the proposed deep convolutional framelets from 48 views. The number on the top right corner represents the NMSE values, and the red arrow refers to the area of noticeable differences. FBP reconstruction results from (a) full projection views, and (b) 48 views. Reconstruction results by (c) CNN, (d) U-net, and (e) the proposed multi-resolution deep convolutional framelets.

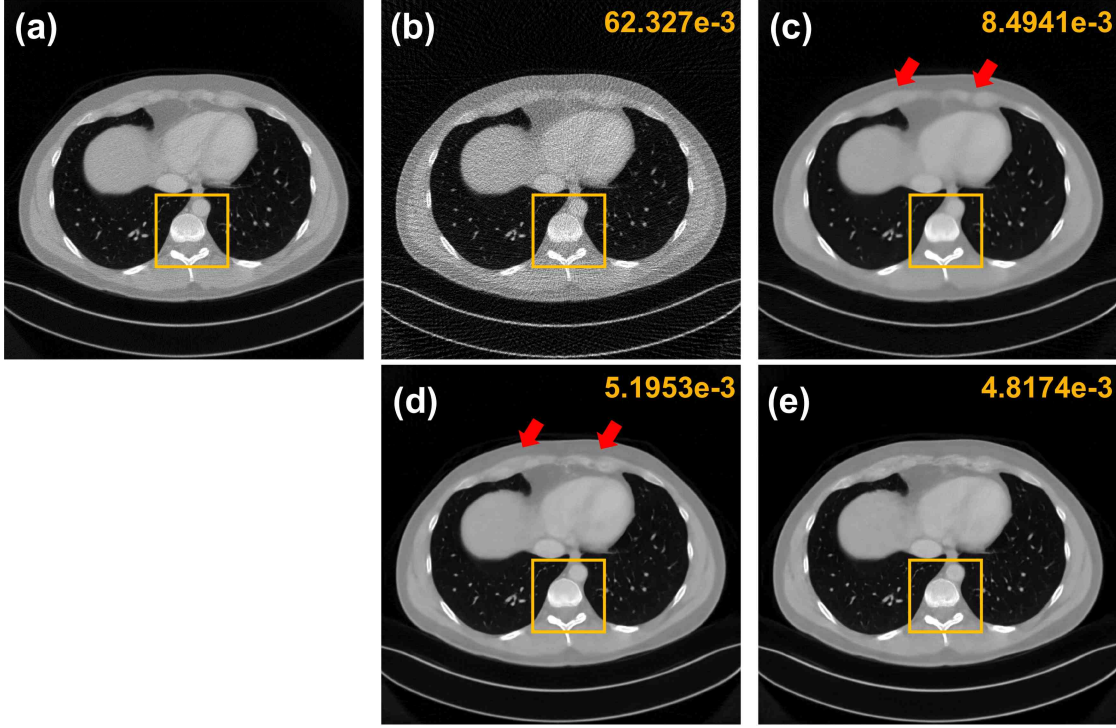


Fig. 14. CT reconstruction results for single scale CNN, U-Net and the proposed deep convolutional framelets from 192 views. The number on the top right corner represents the NMSE values, and the red arrow refers to the area of noticeable differences. The yellow boxes denote the zoomed area in Fig. 15. FBP reconstruction results from (a) full projection views, and (b) 192 views. Reconstruction results by (c) CNN, (d) U-net, and (e) the proposed multi-resolution deep convolutional framelets.

B. Reconstruction results

Due to the high-pass branch of the network to guarantee the PR condition, the deep convolutional framelets produced consistently improved images across all view downsampling factor. Fig. 13(a)-(e) shows reconstruction results from 48 projection views. Due to the severe view downsampling, the FBP reconstruction result in Fig. 13(b) provides severely corrupted images with significant streaking artifacts. Accordingly, all the reconstruction results in Fig. 13(c)-(e) were not compatible to the full view reconstruction results in Fig. 13(a). In particular, there are significant remaining streaking artifacts for the conventional CNN architecture (Fig. 13(c)), which were reduced using U-net as shown in Fig. 13(d). However, as indicated by the arrow, some remaining streaking artifacts were visible in Fig. 13(d). On the other hand, the proposed network totally removes the streaking artifact as shown in Fig. 13(e). Quantitative evaluation also showed that the proposed deep convolutional framelets has the minimum NMSE values.

As for reconstruction results from larger number of projection views, Fig. 14(a)-(e) shows reconstruction results from 192 projection views. All the algorithms significantly improved compared to the 48 view reconstruction. However, the reconstruction results by single resolution CNN in Fig. 15(b) and U-net in Fig.

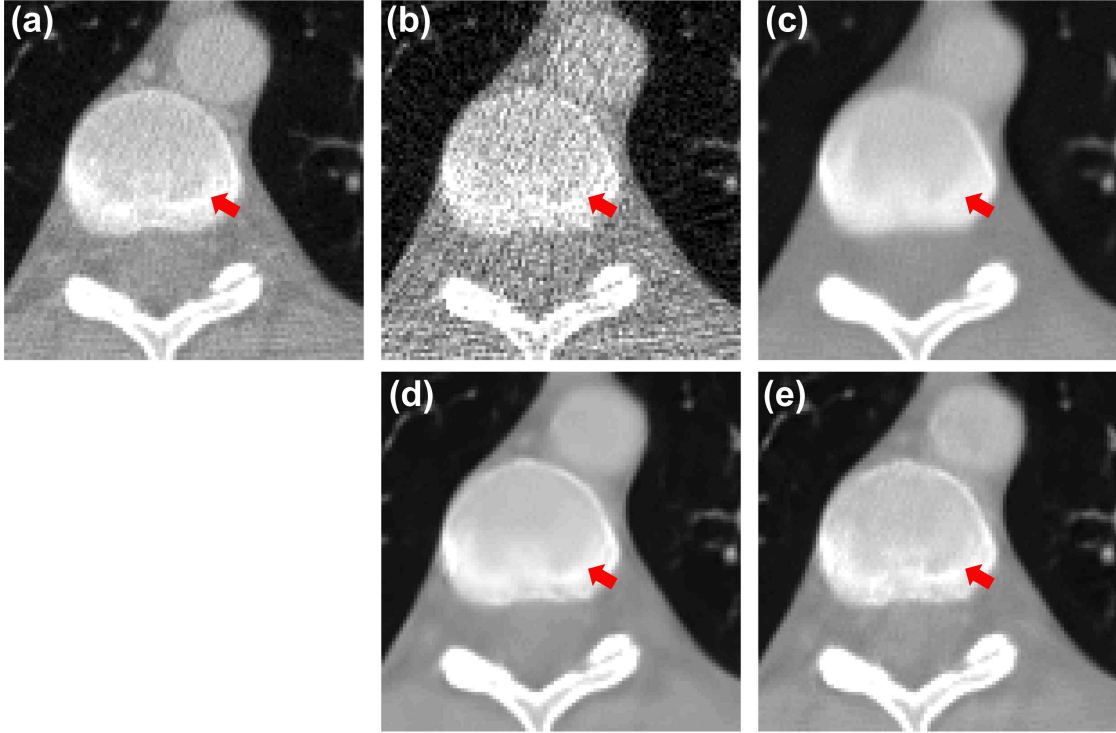


Fig. 15. Zoomed area in Fig.14. FBP reconstruction results from (a) full projection views, and (b) 192 views. Reconstruction results by (c) CNN, (d) U-net, and (e) the proposed multi-resolution deep convolutional framelets.

15(c) are somewhat blurry. On the other hand, most of the edge structures were accurately reconstructed by the proposed deep convolutional framelets as shown in Fig. 14(e). Quantitative evaluation also showed that the proposed deep convolutional framelets has the minimum NMSE values. The zoomed area in Fig. 15(a)-(e) also confirmed the findings. The reconstruction result by the deep convolutional framelets provided very realistic image, whereas the other results are somewhat blurry.

These experimental results clearly confirmed that the proposed network is quite universal in the sense it can be used for various artifact patterns. This is due to the network structure retaining the high-pass band to support PR condition, which automatically adapts the resolutions even though various scale of image artifacts are present.

VI. DISCUSSIONS

While our mathematical theory of deep convolutional framelet was derived for inverse problems, there are many important implications of our finding to general deep learning. For example, we conjecture that the classification network corresponds to a part of our deep convolutional framelets. More specifically, the encoder part of the deep convolutional framelets works for the energy compaction, so the classifier attached to the encoder is basically discriminating the input signals based on the compacted energy distributions. This

is similar with the classical classifier design, where the feature vector is first obtained by a dimensionality reduction algorithm, after which support vector machine (SVM) type classifier is used. Accordingly, the role of the ReLU, residual net, and redundant channels are believed to hold for classifier networks as well.

Another interesting observation is that the perfect reconstruction is directly related to finite sample expressivity of a neural network [55]. Recently, there appeared a very intriguing article providing empirical evidences that the traditional statistical learning theoretical approaches fail to explain why large neural networks generalize well in practice [55]. To explain this, the authors showed that simple depth two neural networks already have perfect finite sample expressivity as soon as the number of parameters exceeds the number of data points [55]. We conjecture that the perfect finite sample expressivity is closely related to the perfect reconstruction conditions, saying that any finite sample size input can be reproduced perfectly using a neural network. The intriguing link between the PR condition and finite sample expressivity needs further investigation.

Finally, one interesting aspect of our convolutional framelet analysis was the increases of filter channels as shown in (28). While this does not appear to follow the conventional implementation of the convolutional filter channels, there is a very interesting article that provides a strong empirical evidence of our theoretical prediction. In the recent paper on pyramidal residual network [56], the authors gradually increase the feature map dimension at all units. This design was proven to be an effective means of improving generalization ability. This coincides with our prediction in (28); that is, in order to guarantee the PR condition, the filter channel should increase. This again suggests the theoretical potential of the proposed deep convolutional framelets.

VII. CONCLUSIONS

In this paper, we propose a general deep learning framework for inverse problems called deep convolutional framelets. Unlike the conventional deep learning approaches that are derived by trial and errors, the proposed network architecture was obtained based on key fundamental theoretical advances we have achieved. First, we show that the deep learning is closely related to the existing theory of annihilating filter-based low-rank Hankel matrix approaches (ALOHA) and convolutional framelets. In particular, our theory was motivated by the observation that when a signal is lifted to a high dimensional Hankel matrix, it usually results in the low-rank structure. Furthermore, the lifted Hankel matrix can be expanded using the so-called convolutional framelets with nonlocal basis convolved with local basis that is usually energy compacting when the underlying Hankel matrix has low rank structure. By extending this idea furthermore, we also derived the perfect reconstruction condition for the deep convolutional framelets. In particular, we showed that the perfect reconstruction is still possible when the framelet coefficients are processed with ReLU. Amazingly,

many of the important aspects of the deep learning such as generalization power, residual blocks, redundant channels and CReLU emerge from the PR condition under ReLU.

Our discovery provided theoretical justification of many existing deep learning architecture for inverse problems but also revealed their limitations. Accordingly, we proposed a novel class of deep network using multi-resolution convolutional framelets combined with ReLU, redundant channels as well as residual blocks. Our numerical results showed that the proposed deep convolutional framelets can provide improved reconstruction performance under various conditions. We believe that our discovery opens a new research direction toward the complete understanding of deep neural network.

VIII. ACKNOWLEDGEMENT

The authors would like to thanks Dr. Cynthia MacCollough, the Mayo Clinic, the American Association of Physicists in Medicine (AAPM), and grant EB01705 and EB01785 from the National Institute of Biomedical Imaging and Bioengineering for providing the Low-Dose CT Grand Challenge data set. This work is supported by Korea Science and Engineering Foundation, Grant number NRF-2016R1A2B3008104.

APPENDIX

The proof is a simple application of the definition of Hankel matrix and convolutional framelet. We prove claims one by one:

- (1) The proof can be found in [30].
- (2) Because $\{A_k\}_{k=1}^n$ constitutes a orthonormal basis, for any $F \in \mathcal{H}(n, d)$, we have

$$F = \sum_{k=1}^n \langle A_k, F \rangle A_k.$$

Furthermore, the operator $\mathbb{H}_d : f \mapsto \mathcal{H}(n, d)$ is linear, so we have

$$\mathbb{H}_d(f) = \mathbb{H}_d \left(\sum_{k=1}^n f[k] e_k \right) = \sum_{k=1}^n f[k] \mathbb{H}_d(e_k) = \sqrt{d} \sum_{k=1}^n f[k] A_k$$

where the last equality comes from (7). Thus, $\langle A_k, \mathbb{H}_d(f) \rangle = \sqrt{d} f[k]$.

- (3) The proof can be found in [29].
- (4) Using (9) and $A_k = \mathbb{H}_d(e_k)/\sqrt{d}$, we have

$$\langle A_k, uv^\top \rangle = \frac{1}{\sqrt{d}} e_k^\top (u \otimes v) = \frac{1}{\sqrt{d}} (u \otimes v)[k].$$

- (5) We need to show that $\mathbb{H}_d^\dagger(\mathbb{H}_d(f)) = f$ for any $f = [f[1] \cdots f[n]]^T \in \mathbb{R}^n$.

$$\mathbb{H}_d^\dagger(\mathbb{H}_d(f)) = \frac{1}{\sqrt{d}} \begin{bmatrix} \langle A_1, \mathbb{H}_d(f) \rangle \\ \langle A_2, \mathbb{H}_d(f) \rangle \\ \vdots \\ \langle A_n, \mathbb{H}_d(f) \rangle \end{bmatrix} = \frac{1}{\sqrt{d}} \begin{bmatrix} \sqrt{d} f[1] \\ \sqrt{d} f[2] \\ \vdots \\ \sqrt{d} f[n] \end{bmatrix} = f$$

where we use $\langle A_k, \mathbb{H}_d(f) \rangle = \sqrt{d} f[k]$.

(6) For $\Phi \in \mathbb{R}^{n \times n}$ and $C \in \mathbb{R}^{n \times d}$ and $\Psi \in \mathbb{R}^{d \times q}$,

$$\mathbb{H}_d^\dagger(\Phi C \Psi^\top) = \sum_{i=1}^q \mathbb{H}_d^\dagger(\Phi c_i \psi_i^\top) . \quad (40)$$

Furthermore, using (11), we have

$$\mathbb{H}_d^\dagger(\Phi c_i \psi_i^\top) = \frac{1}{\sqrt{q}} \begin{bmatrix} \langle A_1, \Phi c_i \psi_i^\top \rangle \\ \langle A_2, \Phi c_i \psi_i^\top \rangle \\ \vdots \\ \langle A_n, \Phi c_i \psi_i^\top \rangle \end{bmatrix} = \frac{1}{q} \begin{bmatrix} (\Phi c_i \otimes \psi_i)[1] \\ (\Phi c_i \otimes \psi_i)[2] \\ \vdots \\ (\Phi c_i \otimes \psi_i)[n] \end{bmatrix} = \frac{1}{q} (\Phi c_i \otimes \psi_i)$$

Thus, we have

$$\mathbb{H}_d^\dagger(\Phi C \Psi^\top) = \frac{1}{q} \sum_{i=1}^q (\Phi c_i \otimes \psi_i) . \quad (41)$$

(7) We need to show that $\mathbb{H}_{d|p}^\dagger(\mathbb{H}_{d|p}(A)) = A$ for any $A = [a_1, \dots, a_p] \in \mathbb{R}^{n \times p}$. Specifically, we have

$$\mathbb{H}_{d|p}^\dagger(\mathbb{H}_{d|p}(A)) = \mathbb{H}_{d|p}^\dagger([\mathbb{H}_d(a_1) \ \dots \ \mathbb{H}_d(a_p)]) \quad (42)$$

where $\mathbb{H}_d(a_i) \in \mathbb{R}^{n \times d}$. Thus, using (13), we have

$$\begin{aligned} \mathbb{H}_{d|p}^\dagger(\mathbb{H}_{d|p}(A)) &= [\mathbb{H}_d^\dagger(\mathbb{H}(a_1)) \ \dots \ \mathbb{H}_d^\dagger(\mathbb{H}(a_p))] \\ &= [a_1 \ \dots \ a_p] = A . \end{aligned}$$

This concludes the proof.

REFERENCES

- [1] A. Krizhevsky, I. Sutskever, and G. E. Hinton, "Imagenet classification with deep convolutional neural networks," in *Advances in neural information processing systems*, 2012, pp. 1097–1105.
- [2] O. Ronneberger, P. Fischer, and T. Brox, "U-net: Convolutional networks for biomedical image segmentation," in *International Conference on Medical Image Computing and Computer-Assisted Intervention*. Springer, 2015, pp. 234–241.
- [3] K. Zhang, W. Zuo, Y. Chen, D. Meng, and L. Zhang, "Beyond a gaussian denoiser: Residual learning of deep CNN for image denoising," *arXiv preprint arXiv:1608.03981*, 2016.
- [4] J. Kim, J. K. Lee, and K. M. Lee, "Accurate image super-resolution using very deep convolutional networks," *arXiv preprint arXiv:1511.04587*, 2015.
- [5] W. Shi, J. Caballero, F. Huszár, J. Totz, A. P. Aitken, R. Bishop, D. Rueckert, and Z. Wang, "Real-time single image and video super-resolution using an efficient sub-pixel convolutional neural network," in *Proceedings of the IEEE Conference on Computer Vision and Pattern Recognition*, 2016, pp. 1874–1883.
- [6] B. Poole, S. Lahiri, M. Raghu, J. Sohl-Dickstein, and S. Ganguli, "Exponential expressivity in deep neural networks through transient chaos," in *Advances In Neural Information Processing Systems*, 2016, pp. 3360–3368.
- [7] M. Telgarsky, "Benefits of depth in neural networks," in *JMLR: Workshop and Conference Proceedings*, 2016, pp. 1–23.
- [8] M. Anthony and P. L. Bartlett, *Neural network learning: Theoretical foundations*. Cambridge university press, 2009.
- [9] P. L. Bartlett and S. Mendelson, "Rademacher and Gaussian complexities: Risk bounds and structural results," *Journal of Machine Learning Research*, vol. 3, no. Nov, pp. 463–482, 2002.
- [10] Y. LeCun, Y. Bengio, and G. Hinton, "Deep learning," *Nature*, vol. 521, no. 7553, pp. 436–444, 2015.
- [11] E. Kang, J. Min, and J. C. Ye, "A deep convolutional neural network using directional wavelets for low-dose x-ray CT reconstruction," *arXiv preprint arXiv:1610.09736*, 2016.
- [12] Y. Chen, W. Yu, and T. Pock, "On learning optimized reaction diffusion processes for effective image restoration," in *Proceedings of the IEEE Conference on Computer Vision and Pattern Recognition*, 2015, pp. 5261–5269.
- [13] X. Mao, C. Shen, and Y.-B. Yang, "Image restoration using very deep convolutional encoder-decoder networks with symmetric skip connections," in *Advances in Neural Information Processing Systems*, 2016, pp. 2802–2810.
- [14] K. H. Jin, M. T. McCann, E. Froustey, and M. Unser, "Deep convolutional neural network for inverse problems in imaging," *arXiv preprint arXiv:1611.03679*, 2016.
- [15] Y. Han, J. Yoo, and J. C. Ye, "Deep residual learning for compressed sensing CT reconstruction via persistent homology analysis," *arXiv preprint arXiv:1611.06391*, 2016.
- [16] S. Wang, Z. Su, L. Ying, X. Peng, S. Zhu, F. Liang, D. Feng, and D. Liang, "Accelerating magnetic resonance imaging via deep learning," in *2016 IEEE 13th International Symposium on Biomedical Imaging (ISBI)*. IEEE, 2016, pp. 514–517.
- [17] K. Hammernik, F. Knoll, D. Sodickson, and T. Pock, "Learning a variational model for compressed sensing MRI reconstruction," in *Proceedings of the International Society of Magnetic Resonance in Medicine (ISMRM)*, 2016.
- [18] K. Kwon, D. Kim, H. Seo, J. Cho, B. Kim, and H. Park, "Learning-based reconstruction using artificial neural network for higher acceleration," in *Proceedings of the International Society of Magnetic Resonance in Medicine (ISMRM)*, 2016.
- [19] Y. S. Han, J. Yoo, and J. C. Ye, "Deep learning with domain adaptation for accelerated projection reconstruction mr," *arXiv preprint arXiv:1703.01135*, 2017.
- [20] I. Daubechies, *Ten lectures on wavelets*. SIAM, 1992.
- [21] D. L. Donoho, "Compressed sensing," *IEEE Trans. on Information Theory*, vol. 52, no. 4, pp. 1289–1306, April 2006.
- [22] E. Candes, J. Romberg, and T. Tao, "Robust uncertainty principles: Exact signal reconstruction from highly incomplete frequency information," *IEEE Trans. on Information Theory*, vol. 52, no. 2, pp. 489–509, Feb. 2006.
- [23] A. Buades, B. Coll, and J.-M. Morel, "A non-local algorithm for image denoising," in *Computer Vision and Pattern Recognition, 2005. CVPR 2005. IEEE Computer Society Conference on*, vol. 2. IEEE, 2005, pp. 60–65.
- [24] K. Dabov, A. Foi, V. Katkovnik, and K. Egiazarian, "Image denoising by sparse 3-D transform-domain collaborative filtering," *IEEE Transactions on image processing*, vol. 16, no. 8, pp. 2080–2095, 2007.
- [25] K. Gregor and Y. LeCun, "Learning fast approximations of sparse coding," in *Proceedings of the 27th International Conference on Machine Learning (ICML-10)*, 2010, pp. 399–406.
- [26] B. Xin, Y. Wang, W. Gao, and D. Wipf, "Maximal sparsity with deep networks," pp. 4340–4348, 2016.
- [27] S. Mallat, *A wavelet tour of signal processing*. Academic press, 1999.
- [28] J. Bruna and S. Mallat, "Invariant scattering convolution networks," *IEEE transactions on pattern analysis and machine intelligence*, vol. 35, no. 8, pp. 1872–1886, 2013.
- [29] R. Yin, T. Gao, Y. M. Lu, and I. Daubechies, "A tale of two bases: Local-nonlocal regularization on image patches with convolution framelets," *SIAM Journal on Imaging Sciences*, vol. 10, no. 2, pp. 711–750, 2017.
- [30] J. C. Ye, J. M. Kim, K. H. Jin, and K. Lee, "Compressive sampling using annihilating filter-based low-rank interpolation," *IEEE Transactions on Information Theory*, vol. 63, no. 2, pp. 777–801, Feb. 2017.
- [31] K. H. Jin and J. C. Ye, "Annihilating filter-based low-rank Hankel matrix approach for image inpainting," *IEEE Transactions on Image Processing*, vol. 24, no. 11, pp. 3498–3511, 2015.
- [32] K. H. Jin, D. Lee, and J. C. Ye, "A general framework for compressed sensing and parallel MRI using annihilating filter based low-rank hankel matrix," *IEEE Trans. on Computational Imaging*, vol. 2, no. 4, pp. 480–495, Dec 2016.
- [33] G. Ongie and M. Jacob, "Off-the-grid recovery of piecewise constant images from few fourier samples," *SIAM Journal on Imaging Sciences*, vol. 9, no. 3, pp. 1004–1041, 2016.
- [34] D. Lee, K. H. Jin, E. Y. Kim, S.-H. Park, and J. C. Ye, "Acceleration of MR parameter mapping using annihilating filter-based low rank hankel matrix (ALOHA)," *Magnetic resonance in medicine*, vol. 76, no. 6, p. 1848?1868, December 2016.
- [35] J. Lee, K. H. Jin, and J. C. Ye, "Reference-free single-pass EPI Nyquist ghost correction using annihilating filter-based low rank Hankel matrix (ALOHA)," *Magnetic resonance in medicine*, vol. 76, no. 8, p. 1775?1789, December 2016.

- [36] K. H. Jin, J.-Y. Um, D. Lee, J. Lee, S.-H. Park, and J. C. Ye, "MRI artifact correction using sparse+ low-rank decomposition of annihilating filter-based hankel matrix," *Magnetic Resonance in Medicine*, 2016.
- [37] M. Fazel, T. K. Pong, D. Sun, and P. Tseng, "Hankel matrix rank minimization with applications to system identification and realization," *SIAM Journal on Matrix Analysis and Applications*, vol. 34, no. 3, pp. 946–977, 2013.
- [38] Y. Hua and T. K. Sarkar, "Matrix pencil method for estimating parameters of exponentially damped/undamped sinusoids in noise," *IEEE Transactions on Acoustics, Speech, and Signal Processing*, vol. 38, no. 5, pp. 814–824, 1990.
- [39] L. Tong, G. Xu, and T. Kailath, "Blind identification and equalization based on second-order statistics: A time domain approach," *IEEE Transactions on Information Theory*, vol. 40, no. 2, pp. 340–349, 1994.
- [40] M. Vetterli, P. Marziliano, and T. Blu, "Sampling signals with finite rate of innovation," *IEEE transactions on Signal Processing*, vol. 50, no. 6, pp. 1417–1428, 2002.
- [41] K. H. Jin and J. C. Ye, "Sparse+ low rank decomposition of annihilating filter-based Hankel matrix for impulse noise removal," *arXiv preprint arXiv:1510.05559*, 2015.
- [42] J. Min, L. Carlini, M. Unser, S. Manley, and J. C. Ye, "Fast live cell imaging at nanometer scale using annihilating filter-based low-rank Hankel matrix approach," in *SPIE Optical Engineering+ Applications*. International Society for Optics and Photonics, 2015, pp. 95 970V–95 970V.
- [43] H. Noh, S. Hong, and B. Han, "Learning deconvolution network for semantic segmentation," in *Proceedings of the IEEE International Conference on Computer Vision*, 2015, pp. 1520–1528.
- [44] D. L. Donoho, "De-noising by soft-thresholding," *IEEE transactions on information theory*, vol. 41, no. 3, pp. 613–627, 1995.
- [45] X. Glorot, A. Bordes, and Y. Bengio, "Deep sparse rectifier neural networks," in *Aistats*, vol. 15, no. 106, 2011, p. 275.
- [46] K. He, X. Zhang, S. Ren, and J. Sun, "Delving deep into rectifiers: Surpassing human-level performance on imagenet classification," in *Proceedings of the IEEE international conference on computer vision*, 2015, pp. 1026–1034.
- [47] ———, "Deep residual learning for image recognition," in *Proceedings of the IEEE Conference on Computer Vision and Pattern Recognition*, 2016, pp. 770–778.
- [48] S. Boyd and L. Vandenberghe, *Convex optimization*. Cambridge university press, 2004.
- [49] N. Ahmed, T. Natarajan, and K. R. Rao, "Discrete cosine transform," *IEEE transactions on Computers*, vol. 100, no. 1, pp. 90–93, 1974.
- [50] W. Shang, K. Sohn, D. Almeida, and H. Lee, "Understanding and improving convolutional neural networks via concatenated rectified linear units," in *International Conference on Machine Learning*, 2016, pp. 2217–2225.
- [51] B. Zhu, J. Z. Liu, B. R. Rosen, and M. S. Rosen, "Image reconstruction by domain transform manifold learning," *arXiv preprint arXiv:1704.08841*, 2017.
- [52] E. Y. Sidky and X. Pan, "Image reconstruction in circular cone-beam computed tomography by constrained, total-variation minimization," *Physics in medicine and biology*, vol. 53, no. 17, p. 4777, 2008.
- [53] D. L. Donoho, "Compressed sensing," *IEEE Transactions on information theory*, vol. 52, no. 4, pp. 1289–1306, 2006.
- [54] A. Vedaldi and K. Lenc, "Matconvnet: Convolutional neural networks for Matlab," in *Proceedings of the 23rd ACM international conference on Multimedia*. ACM, 2015, pp. 689–692.
- [55] C. Zhang, S. Bengio, M. Hardt, B. Recht, and O. Vinyals, "Understanding deep learning requires rethinking generalization," *arXiv preprint arXiv:1611.03530*, 2016.
- [56] D. Han, J. Kim, and J. Kim, "Deep pyramidal residual networks," *arXiv preprint arXiv:1610.02915*, 2016.